Plant Physiology Preview. Published on February 7, 2013, as DOI:10.1104/pp.112.208694

Running Title:

***OsAt10* activation alters rice cell walls**

Corresponding Author:

Professor Pamela C. Ronald

Department of Plant Pathology and The Genome Center

University of California, Davis, CA 95616

and

Joint BioEnergy Institute

5885 Hollis St, Emeryville, CA 94608

tel:(530) 752-1654

email: pcronald@ucdavis.edu

Subject:

Biochemical Processes and Macromolecular Structures

Overexpression of a BAHD Acyltransferase, *OsAt10*, alters rice cell wall hydroxycinnamic acid content and saccharification

Laura E. Bartley[1,2,3], Matthew L. Peck[1], Sung-Ryul Kim[4], Berit Ebert[3,5], Chithra Manisseri[3], Dawn M. Chiniquy[2,3], Robert Sykes[6], Lingfang Gao[1], Carsten Rautengarten[3,5], Miguel E. Vega-Sánchez[2,3,5], Peter I. Benke[3,5], Patrick E. Canlas[2], Peijian Cao[2,3,7], Susan Brewer[2], Fan Lin[1], Whitney L. Smith[8], Xiaohan Zhang[9], Jay D. Keasling[3,5,10], Rolf E. Jentoff[9], Steven B. Foster[8], Jizong Zhou[1], Angela Ziebell[6], Gynheung An[4], Henrik V. Scheller[3,5], Pamela C. Ronald[2,3,4,5]

[1] Department of Microbiology and Plant Biology, 770 Van Vleet Oval, University of Oklahoma, Norman, OK 73019

[2] Department of Plant Pathology and The Genome Center, University of California, Davis, CA 95616

[3] Joint BioEnergy Institute, 5885 Hollis St, Emeryville, CA 94608

[4] Crop Biotech Institute & Department of Plant Molecular Systems Biotech, Kyung Hee University, Yongin 446-701, Republic of Korea

[5] Physical Biosciences Division, Lawrence Berkeley National Laboratory, Berkeley, CA 94720

[6] BioEnergy Sciences Center, National Renewable Energy Laboratory, Golden, CO 80401

[7] China Tobacco Gene Research Center, Zhengzhou Tobacco Research Institute, Zhengzhou, Henan 450001, China

[8] Department of Chemistry and Biochemistry, University of Oklahoma, Norman, OK 73019

[9] Department of Chemical, Biological and Materials Engineering, University of Oklahoma, Norman, OK 73019

[10] Department of Chemical and Biomolecular Engineering, Department of Bioengineering, University of California, Berkeley, CA 94720, USA

Running Title: ***OsAt10* activation alters rice cell walls**

Financial Support: Work at the University of Oklahoma was supported by the National Science Foundation EPSCoR program under Grant No. EPS-0814361. Work conducted by Joint BioEnergy Institute members was supported by the Office of Science, Office of Biological and Environmental Research, of the U.S. Department of Energy under Contract No. DE-AC02-05CH11231. BioEnergy Science Center members were also supported by the Office of Biological and Environmental Research in the DOE Office of Science. R.J. was supported by the National Science Foundation under Grant No. 0923247. Any opinions, findings, conclusions, or recommendations expressed in this material are those of the authors and do not necessarily reflect the views of the funding agencies.

Current Address:

Susan Brewer: DuPont Industrial Biosciences, 925 Page Mill Road, Palo Alto, CA 94304

Corresponding Author:

Professor Pamela C. Ronald

Department of Plant Pathology and The Genome Center

University of California, Davis, CA 95616

and

Joint BioEnergy Institute

5885 Hollis St, Emeryville, CA 94608

tel:(530) 752-1654

email: pcronald@ucdavis.edu

ABSTRACT

Grass cell wall properties influence food, feed, and biofuel feedstock usage efficiency. The glucuronoarabinoxylan of grass cell walls is esterified with the phenylpropanoid-derived hydroxycinnamic acids, ferulic acid (FA) and *para*-coumaric acid (*p*-CA). Feruloyl esters undergo oxidative coupling with neighboring phenylpropanoids on glucuronoarabinoxylan and lignin. Examination of rice (*Oryza sativa*) mutants in a grass-expanded and -diverged clade of BAHD acyl-coenzyme A-utilizing transferases identified four mutants with altered cell wall FA or *p*-CA contents. Here, we report on the effects of overexpressing one of these genes, *OsAt10* (*LOC_Os06g39390*), in rice. An activation-tagged line, *OsAT10-D1*, shows a 60% reduction in matrix polysaccharide-bound FA and a ~300% increase in *p*-CA in young leaf tissue, but no discernible phenotypic alterations in vegetative development, or lignin content or composition. Two additional independent *OsAt10* overexpression lines show similar changes in FA and *p*-CA content. Cell wall fractionation and liquid chromatography-mass spectrometry experiments isolate the cell wall alterations in the mutant to ester conjugates of a 5-carbon sugar with *p*-CA and FA. These results suggest that OsAT10 is a *p*-coumaroyl CoA transferase involved in glucuronoarabinoxylan modification. Biomass from *OsAT10-D1* exhibits a 20 to 40% increase in saccharification yield depending on the assay. Thus, *OsAt10* is an attractive target for improving grass cell wall quality for fuel and animal feed.

Grass biomass is abundant. Grasslands, including those converted to produce the major cereal crops—rice, wheat and maize—cover 20% of terrestrial land (Kellogg, 2001). Resource economists estimate that grass biomass from dedicated bioenergy crops and non-food portions from cultivated cereals represents 57% of the biomass that can be sustainably produced in the U.S. (US-DOE, 2011). Globally, rice straw alone composes 23% of agricultural waste (Lal, 2005).

Cell wall properties impact economic uses of grass biomass and ecosystems. For biofuel production via biochemical conversion, the inefficiency of deconstructing cell walls into their component sugars represents a key production limitation (Lynd et al., 2008). Other uses for grasses and their seeds are also influenced by cell wall composition and structure. Cell wall content influences the efficiency with which animals digest grass forages and feed (Lam et al., 2003; Casler and Jung, 2006). In human foods, the cell wall components of whole grains, such as in whole wheat and brown rice, have beneficial effects on health and various impacts on food processing (Fincher, 2009). Furthermore, grass root and leaf litter compositions affect soil carbon storage (Pendall et al., 2011; Zhou et al., 2012).

In contrast to the primary cell walls of dicotyledonous plants (type I walls), primary cell walls of grasses and other Commelinid monocots (type II walls) consist of up to 40% dry weight of the matrix polysaccharide glucuronoarbinoxylan (GAX) [reviewed in: (Carpita, 1996; Vogel, 2008; Scheller and Ulvskov, 2010)]. Grass GAX is composed of a backbone of ß-1,4-linked xylose residues substituted mostly at the O3 position with arabinofuranose residues and infrequently with glucuronic acid residues (Obel et al., 2006). In contrast, the xylan of dicots is present mostly in secondary cell walls that accumulate after cessation of growth, is infrequently substituted with arabinose, and possess numerous glucuronic and methylglucuronic acid residues. Another unique aspect of the GAX of grasses and other monocots with type II walls is that a fraction of the arabinose residues are substituted at the O5 position with the hydroxycinnamic acid, ferulic acid (FA, Figure 1A) [reviewed in (Buanafina, 2009)]. Dehydrodimers of ferulate (diferulates) form through oxidative coupling likely mediated by peroxidases (Takahama and Oniki, 1994; Bunzel et al., 2008) and cross-link adjacent xylan strands to one another (Ishii, 1991; Allerdings et al., 2005). Furthermore, the observation of ether linkages between ferulate and monolignols suggests that ferulic acid on GAX may nucleate lignin polymerization (Bunzel et al., 2004).

Another hydroxycinnamate, *para*-coumaric acid (*p*-CA, Figure 1A), is also ester-linked to components of grass cell walls. *p*-Coumaroyl esters are abundant on lignin, but also esterify grass GAX (Mueller-Harvey et al., 1986; Ishii et al., 1990; Saulnier et al., 1995; Faulds et al.,

2004; Ralph, 2010). Though *p*-CA is readily oxidized to its radical, *p*-CA dimers have not been observed *in planta* (Ralph et al., 1994). Rather *p*-coumaroyl substituents may act as "radical catalysts," rapidly passing the radical to sinapyl alcohols and facilitating lignin polymerization (Takahama and Oniki, 1994; Ralph, 2010).

FA on GAX, and especially diferulates, are thought to act to strengthen primary and secondary cell walls. Diferulate accumulation correlates with cessation of grass leaf elongation and addition of FA to rice internodes blocks their expansion (MacAdam and Grabber, 2002; Sasayama et al., 2011). Several researchers have observed that ferulate esters in grass biomass block digestibility. FA is inversely correlated with enzymatic sugar release parameters *in vitro* (Grabber et al., 1998; Grabber et al., 1998; Lam et al., 2003; Casler and Jung, 2006). Digestibility inversely correlates with FA and diFA amounts in canarygrass and ryegrass accessions (Lam et al., 2003; Casler and Jung, 2006). In addition, cell wall-associated diferulates and free and cell wall-associated FA and *p*-CA appear to deter fungal pathogens and insect pests of grasses (Santiago et al., 2007; Santiago et al., 2008; Lanoue et al., 2009).

Despite their importance, the proteins that incorporate hydroxycinnamates into grass cell walls have only begun to be characterized. In 2007, Mitchell et al. proposed that a subclade of proteins with the Pfam domain, PF02458, for which transcripts are more abundant in grasses relative to dicots, might incorporate FA into grass walls. PF02458 domain-containing proteins are CoA-acyl dependent acyltransferases present in plants, fungi, and a few bacteria. In plants, these enzymes have been named BAHD acyltransferases, based on the first biochemically characterized family members. They catalyze the addition of an acyl group from the thioester of coenzyme A to oxygen and nitrogen nucleophiles of diverse acceptor molecules in specialized plant metabolism, including volatile esters, anthocyanins, and flavonoids [reviewed in: (Dudareva and Pichersky, 2000; D'Auria, 2006)].

There are well over 50 BAHD members in most sequenced vascular plants (Table I). The BAHD enzymes group robustly into five clades (D'Auria, 2006), though more recently subclades have been proposed (Tuominen et al., 2011). Several characterized members use hydroxycinnamoyl-CoAs as substrates, including the hydroxycinnamoyl-CoA:shikimate/quinate hydroxycinnamoyltransferase (HCT) involved in synthesis of lignin precursors (Hoffmann et al., 2003) and sinapoyl and coumaroyl spermidine transferases (SDT and SCT, respectively, (Luo et al., 2009). Other recent reports have described Arabidopsis suberin and cutin feruloyl transferases and a wax fatty alcohol caffeoyl transferase all of which transfer hydroxycinnamoyl-CoA to ω-hydroxy fatty acid acceptors that accumulate in the extracellular matrix (Molina et al., 2009; Kosma et al., 2012; Rautengarten et al., 2012). Other BAHD enzymes catalyze the

addition of esters to sugar acceptors, such as those that are part of anthocyanins (Unno et al., 2007).

Recent work has provided support for the hypothesis that the BAHD acyltransferase subclade identified by Mitchell, hereafter the "Mitchell clade", is involved in cell wall modification. Withers et al. (2012) described the biochemical characterization of one member of the "Mitchell clade", PMT or here referred to as OsAT4, which possesses *p*-coumarate monolignol acyltransferase activity *in vitro*. Furthermore, Piston et al. (2010) found that rice plants with reduced expression of genes from the "Mitchell clade" exhibited reduced FA in leaves. In that study, plants were engineered with a long inverted repeat silencing construct that targeted conserved regions of the genes that we refer to here as *OsAt6* through *OsAt10*. The authors observed 2- to 3-fold reductions in gene expression and an average 20% reduction in cell wall FA content in the leaves of progeny from two independent transgenic events. Because of the small effect on FA accumulation and the nonspecific nature of the construct, Piston et al. were not able to determine the function of the silenced gene products.

Here, we report that the "Mitchell clade" of BAHD acyltransferases is expanded and diverged in grasses relative to eudicots and non-spermatophyte species. We find that rice mutants with altered expression of four of these genes have altered cell wall hydroxycinnamate content. In-depth characterization of ectopic expression lines for one gene, *OsAt10*, revealed that this modification increases matrix polysaccharide-associated ester-linked *p*-CA while simultaneously decreasing matrix polysaccharide-associated FA. *OsAt10* overexpression plants exhibit increased *in vitro* saccharification, with no discernible effects on vegetative development. Thus, this gene is a useful target for improving biofuel and feed production.

RESULTS

The "Mitchell Clade" of BAHD Acyltransferases is Expanded and Diverged in Grasses

Mitchell et al. (2007) identified what we term the "Mitchell clade" of BAHD acyl-CoA dependent acyltransferases on the basis of high gene expression in grasses relative to dicots. To refine the hypothesis that these enzymes might be involved in grass-diverged cell wall synthesis, we systematically characterized the distribution of this clade in selected plant species and compared the clade with other characterized BAHD proteins. We identified BAHD proteins from the genomes of a diverse set of sequenced plant species available at the time of the analysis and analyzed the phylogenetic relationships among them and a reference set of BAHDs (Table I). To gain higher sensitivity relative to local sequence alignment (i.e., BLAST) for

recognizing sequences with low, but potentially still significant, homology, we used a hidden Markov model to identify putative BAHD proteins (Finn et al., 2011). We then inferred an initial model of the phylogenetic relationships among the putative BAHD proteins from each genome and the set of biochemically characterized BAHD proteins cataloged by D'Auria (2006). While we are aware that recent analyses have included the presence of a strict HXXXD motif as indicative of whether the protein is an active BAHD (Banks et al., 2011; Tuominen et al., 2011), we have included proteins with single amino acid alterations to this motif since one of the known biochemically active proteins for the family involved in taxol biosynthesis, BAPT (NCBI ID: AAL92459, Walker et al., 2002), possesses a variation of this motif in which the histidine is replaced by a serine.

As observed by Tuominen et al. (2011), the distribution of BAHD proteins varies among species (Table I, Supplemental Figure 1). The "Mitchell clade" is embedded within Clade V, or Clade Va of Tuominen et al. (2011). Further, we find that the "Mitchell clade" includes a biochemically characterized banana alcohol CoA acyltransferase, BanAAT (Beekwilder et al., 2004), and is related to a group of BAHD proteins that participate in taxol biosynthesis (Figure 1B and Supplemental Figure 1).

We also conducted a more in-depth analysis of clade V BAHD proteins. We found that multiple proteins with similarity to the rice "Mitchell clade" are present in the grasses, *Sorghum bicolor* and *Brachypodium distachyon* (Table I, Supplemental Fig. 1). In contrast, the annotated proteomes of dicots, *Arabidopsis thaliana*, *Glycine max*, and *Medicago truncatula*, encode only one or two proteins closely related to this clade. While, similar sequences are entirely absent from the annotated proteins of *Populus trichocarpa* and the non-spermatophyte plants, *Selaginella* and *Physcomitrella*. Among characterized Arabidopsis proteins, the most closely related biochemically characterized proteins are the spermidine hydroxycinnamoyl transferases, SCT and SDT (Supplemental Figure 1; (Luo et al., 2009). The recently discovered, cutin, wax, and suberin hydroxycinnamoyl transferases (Molina et al., 2009; Kosma et al., 2012; Rautengarten et al., 2012), though part of clade V, are not part of, or even closely related to the "Mitchell clade". In summary, the "Mitchell clade" appears to be conserved and expanded in grasses relative to dicotyledonous and non-spermatophyte plants. This is consistent with this clade functioning in aspects of Commelinid metabolism that diverge from metabolism of other plants, such as synthesis of type II cell walls.

The analysis described above also revealed that the "Mitchell clade" of BAHD acyltransferases included more proteins than originally recognized. Instead of comprising 12 members in rice (Mitchell et al., 2007; Piston et al., 2010), the group consists of 20 closely

related members that are further subdivided into two subclades (i and ii, Figure 1B). In rice, the 10 genes in subclade i are all supported by expressed sequence tag (EST)-evidence and are relatively highly expressed; whereas, only 7 of the 10 members of subclade ii have been EST-validated, and they are relatively weakly expressed compared with subclade i members (Figure 1B). In addition, the multi-species tree reveals that most proteins of subclade i are represented in all three grass species examined and are more similar to the non-grass proteins (Supplemental Figure 1). In contrast, subclade ii contains more species-specific expansions and/or contractions. To facilitate communication about the "Mitchell clade" acyltransferases, we have given the clade members of rice preliminary names with the format *Oryza sativa* acyltransferase, OsAT1 through OsAT20. As mentioned previously, OsAT4 was recently named PMT and found to be capable of esterifying monolignols (Withers et al., 2012).

Screen of Rice Mutants for Altered Cell Wall Hydroxycinnamic Acid Content

To test the hypothesis that members of the "Mitchell clade" of BAHD CoA acyltransferases are involved in incorporation of FA into grass cell walls, we screened rice mutants with altered expression of these genes and assessed their cell wall characteristics. Supplemental Table II describes the mutant lines we characterized. To complement the work of Piston et al., we particularly, but not exclusively, focused on putative activation tagged lines from the South Korean collection (An et al., 2005; Jeong et al., 2006). We used line-specific PCR primers designed to distinguish the presence and absence of each T-DNA insert to screen 17 putative T-DNA mutant lines putatively targeting 12 of the 20 acyltransferase genes. We did not detect an insert in four lines, and for two lines, did not identify any segregants that were homozygous for the insert out of 20 analyzed offspring (Supplemental Table II).

For the remaining 11 lines, we characterized the alkali-labile hydroxycinnamoyl ester content of cell wall alcohol insoluble residue (AIR) from leaf blades and sheaths of side tillers. We compared homozygous, mutant and wild-type segregant plants seven or ten weeks after planting. The screen revealed four mutants with possible cell wall hydroxycinnamic acid phenotypes (Figure 2, Supplemental Table II). All four lines showed changes in the expression of the nearest acyltransferase gene to the T-DNA insertion site via qRT-PCR (Supplemental Table II). Three of the phenotypes were in putative mutants of subclade i proteins, and one was a mutant in a subclade ii protein. Specifically, homozygous mutant progeny of *2A-20021*, which increases expression of *OsAt5*, exhibited a significant change in the ratio of FA to *p*-CA. In addition, homozygous mutant progeny of *2A-40095*, which carry an insertion that interrupts the end of the coding sequence for *OsAt7*, exhibited reduced FA in leaf sheaths (~60% less). The

location of the T-DNA insertion truncates the *OsAt7* mRNA and, consequently, despite the presence of a transcriptional activator sequences, reduces *OsAt7* mRNA expression. In line *2A-40095*, the 5' of the transcript was reduced by approximately 4-fold.. The 3' end was reduced approximately >5000-fold compared to the wild-type segregant. Furthermore, homozygous mutant progeny of *4A-03423* (hereafter, *OsAT10-D1*), which has increased expression of *OsAt10*, exhibited reduced FA (~60% less) and an increase in *p*-CA (~300% more) in sheaths and leaves. Lastly, homozygous mutant progeny of *1B-00523*, which has increased expression of *OsAT15*, a subclade ii member, exhibited reduced FA in leaves relative to wild-type segregants (~60% less). The other lines we examined showed no significant changes in FA or *p*-CA in the developmental stages and organs examined, and we did not test gene expression in those lines.

Gene Expression and Developmental Phenotypes of *OsAT10-D1*

The T-DNA insertion site for the line we refer to as *OsAT10-D1* (*PFG_4A-03423*) is approximately 8.5 kb downstream of the transcriptional start site for *OsAt10* (Figure 3A). The insert is oriented with the activating sequences proximate to *OsAt10* and in the range observed to activate expression (Jeong et al., 2006). As mentioned above, RT-qPCR indicated that indeed the expression of *OsAt10* was increased by >100-fold in the leaves of homozygous *OsAT10-D1* plants (Figure 3B). In *OsAT10-D1*, besides *OsAt10* the expression of other genes proximate to the site of the T-DNA insertion does not vary significantly relative to the wild type (Figure 3B). Similarly, the expression of related *OsAt* genes does not vary significantly in *OsAT10-D1* (Supplemental Figure 2), reducing the possibility that the observed phenotype is due to compensation at the level of gene expression of a related acyltransferase. Of the acyltransferase transcripts examined in this survey, *OsAt6* appears to vary the most, though not significantly. However, *OsAt6* (*LOC_Os01g08380*) is expressed near the lower limit of our detection and in fact, was reported as undetectable in a previous qRT-PCR study (Piston et al., 2010).

OsAT10-D1 lines show no change in size and dry mass at maturity (Figure 4A & 4B). However, we did measure a ~20 to 30% decrease in total seed mass per plant for the mutant compared to the wild type (Figure 4C).

Cell Walls of *OsAt10* Overexpression Lines have Heritable Alterations in Ester-linked Hydroxycinnamic Acids

For *OsAT10-D1*, we confirmed the inheritance of the altered cell wall hydroxycinnamate phenotype in young leaves and mature tillers of plants from two additional generations (Figure 5 and Supplemental Figure 3). This line reliably exhibits a ~50% decrease in ester-linked FA in young leaf tissue (Figure 5A). The same tissue shows a ~300% (i.e., 3-fold) increase in ester-linked *p*-CA (Figure 5B). The change in both components is most clearly displayed as a change in the ratio of FA to *p*-CA (Figure 5C), which is independent of potential variation in the absolute amounts due to variation in sample mass and extraction efficiency. In addition, we found similar trends, but less extreme changes, in pools of total aerial tissues harvested after senescence for the plants from each genotype (Figure 5). These mature straw samples possess ~40% less FA and ~80% more *p*-CA compared to the wild type. The difference in the magnitude of the effect on *p*-CA in juvenile vs. mature organs may be due to an accumulation of *p*-CA in a cell wall fraction of mature tissues, such as lignin (Ralph, 2010), that is unaffected by increased OsAT10 expression.

We also quantified the four most abundant diferulates. Though signals were near the level of detection for most dimer species, the most abundant dimer, 8-O-4, clearly decreases significantly compared to wild-type amounts (Figure 5D). Moreover, the sum of the dimers shows a highly significant decrease relative to the sum of all the ester-linked hydroxycinnamates in both mutant families examined (Figure 5D). We found that the sum of the diferulates decreases proportionally to the decrease in FA, so that there is no change in the ratio of FA to dimer in the mutant relative to the wild type (Figure 5D).

To gather further evidence that the phenotype in the activation tagged line was due to ectopic expression of *OsAt10*, we generated additional *OsAt10* overexpression lines utilizing the maize *ubiquitin1* promoter (Ubi_{pro}, Figure 6B, Supplemental Figure 4). Contrary to our typical experience for high efficiency transformation with the *japonica* cultivar, *Kitaake* (Jung et al., 2008), we were only able to regenerate from tissue culture two independent transformants that possess the transgene (Figure 6B). This result suggests that the *OsAt10* construct interferes with transformation efficiency. In young leaf blades of plants that were harvested approximately one month following tissue culture regeneration, both of the confirmed transgenic lines show increased expression of *OsAt10*, a dramatic change in the ratio of FA to *p*-CA, and no change in the ratio of FA dimers to FA compared to the non-transgenic “escape” lines (Figure 6B). The low hydroxycinnamate levels in these plants (~10- to 30-fold less than young leaves in Figure 5), may be due the recent calli regeneration. We also characterized segregating progeny of Ubi_{pro}*:OsAt10-4* (Supplemental Figure 4). Young leaf tissue from Ubi_{pro}*:OsAt10-4* express *OsAt10* ~3000-fold more than wild-type segregants. Mature straw from the Ubi_{pro}*:OsAt10-4*

progeny displayed a similar cell wall phenotype to *OsAT10-D1* mature straw. Specifically, *Ubi$_{pro}$:OsAt10* mature straw exhibits a 45% increase in *p*-CA and a 20% decrease in FA compared with straw from wild-type segregants (Supplemental Figure 4).

The Difference in *OsAT10-D1* Hydroxycinnamates is Predominantly TFA-Soluble and is Linked to a 5-Carbon Sugar

In grass cell walls, hydroxycinnamates are predominantly esterified to GAX and to lignin. To determine which cell wall fraction is altered in the *OsAT10-D1* mutant, we subjected AIR from mutant and wild-type mature rice straw to a mild, 50 mM trifluoroacetate (TFA) treatment to cleave acid-labile glycosidic bonds within the matrix polysaccharides (Saulnier et al., 1995; Obel et al., 2003). Within thirty minutes, 50 mM TFA treatment of maize bran cleaved 70% of the α(1-3) xylose-arabinosyl bonds, including arabinose residues esterifed to ferulate (Saulnier et al., 1995). Cleavage of other glycosidic bonds, such of those of the xylan backbone proceeded with slower kinetics. Following acid hydrolysis, we saponified the TFA-supernatants and remaining pellets and analyzed the products with HPLC. The results demonstrate that the alteration in FA and *p*-CA amounts in *OsAT10-D1* is primarily in the matrix polysaccharide fraction of the cell wall (Figure 7). For both the wild type and *OsAT10-D1*, the FA is predominantly associated with the TFA fraction, with less than 20% of FA remaining in the pellet for both genotypes (Figure 7A). The reverse is observed for the *p*-CA for the wild type, for which ~70% of the *p*-CA remains in the pellet (Figure 7B). The mutant has a similar absolute amount of *p*-CA in the pellet, but a lower percentage (~55%). Instead, the additional *p*-CA and reduced FA amounts in the cell wall of the *OsAT10-D1* are in the TFA-soluble matrix polysaccharide fraction. This can be clearly seen in the ratio plot, in which the ratio of FA to *p*-CA is most drastically different in the supernatant after prolonged TFA treatment (Figure 7C). Indeed, the change in *p*-CA in the matrix polysaccharide fraction for mature rice straw approaches the ~300% increase observed for young leaves. Because the lignin-associated *p*-CA fraction is unaffected by the polysaccharide modification, the observation that the modified cell wall constituent is part of the polysaccharide fraction is consistent with the “dilution” of the mutant effect in mature straw for *OsAT10-D1* and *Ubi$_{pro}$:OsAt10-4* plants that have accumulated *p*-coumarylated lignin relative to young leaves (Figure 5 and Supplemental Figure 4).

Further analysis of the TFA-solublized cell wall hydroxycinnamates with electrospray ionization LC-MS strongly supports the hypothesis that GAX is modified by *OsAt10* activation. For this experiment, we compared TFA-hydrolyzed AIR with and without saponification. The TFA-solubilized extract had two major new ion peaks that were absent in the saponified extract

and in hydroxycinnamate standards (Figure 8A). The mass spectra of the these peaks are consistent with the major unknown peak in the mutant (unknown peak 1) consisting of *p*-CA esterified to a five-carbon sugar (m/z of major ion = 295.0285, Figure 8B); whereas, the predominant peak in the wild type (unknown peak 2) contains FA esterified to a five carbon sugar (m/z of major ion = 325.093, Figure 8C). Because arabinose and xylose have the same molecular weight, they are indistinguishable in this experiment; however, our strong expectation is that the esterified sugar is arabinose. Relative quantification of the ion counts of each of these peaks in the mutant vs. the wild type is consistent with the results measured via UV detection. That is, compared with the wild type, *OsAT10-D1* has ~4.6-fold more *p*-CA-sugar and 2.5-fold less FA-sugar (Figure 8A). The relative amounts of FA and *p*-CA after saponification are also consistent with the HPLC data (Figure 8A).

The *OsAT10-D1* Line has an Increase in Cell Wall Glucose Content

Compensatory changes are often seen among the components of the cell wall (Humphrey et al., 2007). Quantification of sugars released by acid treatment of destarched (ds) AIR preparations from mature straw suggests that the glucose content is increased by ~20% (weight/weight) for the mutant relative to the wild type (Figure 9A). We observed the difference both with TFA treatment, which liberates monosaccharides derived from matrix polysaccharides and amorphous cellulose, and when the TFA residue was further treated with sulfuric acid, which breaks down crystalline cellulose (Figure 9A). The difference in the mutant compared to the wild type is most apparent when the products of both treatments are summed together, which gives an increase in glucose in the mutant compared with the wild type of 19% ± 11%. By mass, we did not observe any other significant changes in sugar amounts in the mutant compared to the wild type (Supplemental Figure 5). We also observed no change in the total mass% of sugars in AIR. When the TFA-solubilized sugars are expressed in terms of mol%, the data also indicate an increase in glucose content 11% ± 5% (Figure 9B). The sum of the mol% of other measured sugars (i.e., xylose, arabinose, and the sum of minor sugars) decreases proportionally to the glucose increase (7% ± 7%). This balance in mol% change suggests that the change in polysaccharide content in the mutant is isolated to the glucose-containing polymers.

The *OsAT10-D1* Line Shows No Alterations in Lignin Content or Composition

To further explore the extent of cell wall changes in *OsAT10-D1* relative to wild type, we measured lignin content and composition. We hypothesized that alteration in pools of

hydroxycinnamyl-CoA adducts in the *OsAT10-D1* line might lead to alterations in lignin amount or content, in terms of syringyl (S), guiacyl (G), and hydroxyphenyl (H) subunits. Due to the presence of H residues in grass lignin, all methods of lignin analysis are not equally accurate for grasses relative to dicots. For our analysis, we used two methods suitable for grasses – acetylbromide solubilization (Grabber et al., 1996; Fukushima and Hatfield, 2004) and pyrolysis-molecular beam mass spectrometry (py-MBMS; Evans and Milne, 1987; Agblevor et al., 1994). "Lignin" analyses of whole tissue or AIR typically include all classes of phenylpropanoids, both esterified and non-esterified, though many hydroxycinnamates are esterified to polysaccharides. Since our previous analysis had established a difference in ester-linked phenolics in the mutant, we quantified lignin content and composition with and without removing esterified hydroxycinnamates with saponification.

OsAT10-D1 mature straw samples show no significant differences in the content of acetylbromide soluble lignin after saponification relative to the wild type (Table II). We obtained a similar result via py-MBMS for mature straw and separate, young leaf and sheath samples. The py-MBMS also revealed no difference in the S:G lignin ratio in the mutant compared to the wild type after saponification (Table II). We also collected py-MBMS data for unprocessed straw and AIR of *OsAT10-D1*. Separate analysis of the saponified and unsaponified samples reveals distinctions between the wild type and mutant in the unsaponified samples (Figure 10A). Principle component 1 (PC1) explains the alcohol extraction (30% of the variation) and principle component 2 (PC2) explains the differences between wild-type and mutant samples (19% of the variation). The loadings for PC2 show that the major ions that distinguish wild-type and mutant samples are phenolics (Figure 10B). The MS fragmentation pattern is consistent with an interpretation in which there is an increase of *p*-CA, as reflected by peaks 120, 94, and 91, and a decrease in ferulic acid, as reflected in the reduction in the coniferyl ion, peak 150 (Evans and Milne, 1987). Because principle component analysis no longer distinguishes the samples after saponification (Figure 10C), the observed differences in phenylpropanoids between *OsAT10-D1* and the wild type are likely associated with ester-linked hydroxycinnamates and not lignin, consistent with the other results.

A limitation of the pyrolysis method for determining lignin composition is that it inaccurately measures H-lignin, which volatilizes poorly and instead turns to char upon heating. Because of the increase in *p*-CA, a precursor of H-lignin, in *OsAT10-D1* cell walls relative to the wild type, we sought to determine whether there is a change in the char content of *OsAT10-D1* using a thermogravimetric (TG) pyrolysis instrument. Duplicate runs per genotype of the TG did not detect a difference in the mass remaining from mature straw after pyrolysis (Supplemental

Figure 6), again consistent with there being no difference in core lignin composition or content between *OsAT10-D1* and the wild type.

The *OsAT10-D1* Line Shows an Increase in Saccharification

Ferulate in grass biomass is inversely correlated with digestibility across diverse grass accessions [e.g., (Lam et al., 2003; Casler and Jung, 2006)]. The phenotype of the *OsAT10-D1* line provided the opportunity to determine whether there is also an increase in enzymatic digestibility with reduced FA content when comparing two near-isogenic plant lines. We found that destarched AIR after mild pretreatment followed by incubation with a cellulase cocktail resulted in the release of approximately 20% more reducing sugar from the mutant compared with the wild type at each time point examined (Figure 11A).

We also determined if the improvement in digestibility impacted a biological saccharification agent. For this, we exposed coarsely chopped, acid-pretreated rice straw of the wild type and *OsAT10-D1* to the mesophilic fungus, *Penicillium sp.* YT02. This recently characterized fungus shows significantly higher xylanase and β-glucosidase activities with various insoluble lignocellulosic substrates compared with the commonly used fungal strain, *Trichoderma reesei* (ATCC 24449; Kovacs et al., 2009; LG and JZ, unpublished). In the fungal treatments, the biomass-derived sugars initially accumulate, but are gradually depleted via incorporation into fungal biomass. Qualitatively consistent with the enzymatic deconstruction results, YT02 incubation released 46% more glucose, 82% more xylose, and 25% more arabinose into the medium from *OsAT10-D1* straw than from wild-type straw (Figure 11B, Supplemental Table III). Averaged over the entire time course (12 to 120 hours), the improvement in yield is more dramatic with the fungus than with the simple enzymatic treatment, with a total sugar yield increase of ~40%. Cellulase and ß-glucosidase enzymatic activities in the slurry are unchanged on the mutant straw (Figure 11C and Supplemental Figure 7), suggesting that the fungus grew similarly on both. In contrast and of relevance to the nature of the change caused by the increased expression of *OsAt10*, xylanase activity is dramatically enhanced, especially at later time points (Figure 11C).

DISCUSSION

Hydroxycinnamoyl esters in cell walls influence basic and applied plant traits including growth properties, disease resistance, and food and feed quality (Santiago et al., 2007; Buanafina, 2009). The molecular details of incorporation of hydroxycinnamates into cell walls remain largely obscure. Here, we present results showing that overexpression of *OsAt10* in the

OsAT10-D1 line decreases FA and increases *p*-CA in leaf blades, leaf sheaths, and mature straw (Figure 5). We have also confirmed that overexpression of *OsAt10* in two other independent lines, *Ubi$_{pro}$:OsAt10-4* and *Ubi$_{pro}$:OsAt10-5*, alters the ratio of FA to *p*-CA in a manner similar to *OsAT10-D1* (Figure 6).

Uneven Distribution of BAHD CoA Acyltransferases across Plants

OsAT10 belongs to a grass-diverged and expanded clade of BAHD acyl CoA-utilizing acyltransferase proteins that were originally identified due to their high expression in grasses relative to dicots (Mitchell et al., 2007). Our phylogenetic analysis shows that, with the exception of that of poplar, the genomes of the angiosperms we examined have annotated proteins within the "Mitchell clade". However, compared to 0-2 members in dicotyledenous and non-spermatophyte species, the grasses examined possess genes encoding 12-20 of these proteins (Table 1, Supplemental Figure 1). The presence and expression of a protein in the "Mitchell clade" in banana, BanAAT (Beekwilder et al., 2004), is consistent with the presence of hydroxycinnamates in cell walls of banana, a Commelinid monocot (Carpita, 1996).

Mutant lines for the most closely related Arabidopsis protein, AT3G62160, were recently examined for changes in hydroxycinnamate content of the cell wall and other extracellular polymers; no differences were identified (Rautengarten et al., 2012; CR and HVS, unpublished). Though the function of the Arabidopsis protein remains to be determined, that result is consistent with a model of neofunctionalization or subneofunctionalization of the "Mitchell clade" of BAHD acyltransferases in Commelinid monocots (He and Zhang, 2005). In this model, a duplicated "Mitchell clade" member in the progenitor of Commelinids acquired the ability to modify a cell wall-related substrate. Additional gene duplication events then led to further increases in the number of members of the "Mitchell clade", especially those in subclade i. The conservation of subclade i "Mitchell clade" members across the grasses (Table I and Supplemental Figure 1) is consistent with selection for the retention of their function(s). As will be discussed further below, the different overexpression phenotypes of mutants for different "Mitchell clade" members as well as evidence from the literature is consistent with members of this clade having evolved different specificities.

The Cell Wall Target of OsAT10 is Glucuronoabinoxylan

Previous results have found that *p*-coumaroyl esters are predominantly bonded to lignin; whereas, FA is largely esterified to GAX. However, enzymatic release experiments have provided some prior evidence that *p*-CA is also incorporated into the polysaccharides of grass

cell walls (Mueller-Harvey et al., 1986; Ishii et al., 1990; Faulds et al., 2004). Hydroxycinnamoyl esters are also present in other less abundant components of the cell wall fraction, including suberin, cutin, and waxes (Molina et al., 2009; Schreiber, 2010; Kosma et al., 2012; Rautengarten et al., 2012). We find that mature rice straw has ~20% of *p*-CA associated with matrix polysaccharide (Figure 7). This is likely the major location of the *p*-CA in the young leaf tissue, which we expect to have very low lignin amounts (Figure 5) and incompletely developed cutin and wax layers (Richardson et al., 2007). We found that the hydroxycinnamic acid changes in *OsAT10-D1* are predominantly on the TFA-soluble matrix polysaccharide fraction, not the acid-resistant lignin fraction (Figure 7). Indeed, we were able to confirm that hydroxycinnamoyl moieties in the TFA-released fraction are ester-linked to a 5-carbon sugar (Figure 8). Since the sugar-hydroxycinnamoyl species migrate in narrow windows in the LC-MS analysis, it is most likely that the fractions represent only arabinose esters, which have been frequently described (Mueller-Harvey et al., 1986; Saulnier et al., 1995; Buanafina, 2009). Though a formal possibility, it is unlikely that this peak also contains feruloylated-xylose, which has only been described from bamboo xyloglucan (Ishii et al., 1990). Furthermore, we have no evidence to suggest that OsAT10 functions as a *p*-CA monolignol acyltransferase, which has been described in recent publications (Hatfield et al., 2009; Withers et al., 2012). Rather, it seems likely that the native function of OsAT10 is to incorporate *p*-CA into a precursor of GAX.

How OsAT10 can mediate transfer of *p*-CA to xylan is a conundrum since all the BAHD enzymes to date have been found to be cytoplasmic (D'Auria, 2006); whereas, xylan synthesis takes place inside the Golgi lumen (Oikawa et al., 2012). One possibility is that OsAT10 transfers *p*-CA to UDP-arabinofuranose, which is formed by UDP-arabinose mutase located on the cytoplasmic side of the Golgi (Rautengarten et al., 2011). Buanafina (2009) proposed such a reaction mechanism, but no direct biochemical evidence has been demonstrated. Biochemical analysis of wheat lysates revealed transient feruloylation of a 40 kDa protein (Obel et al., 2003). Although the protein was not identified, the observation is consistent with UDP-arabinose mutase functioning as an intermediate.

Another observation for which the mechanism remains to be determined is the decrease in sugar-feruloylation that accompanies the increase in polysaccharide *p*-coumaroylation in *OsAt10*- overexpressing plants. Specificity in the frequency of substitution of arabinose, such that FA and *p*-CA substituents are in partial competition, may account for this observation. Alternatively or in addition, since *p*-CA is a precursor of FA, the increased activity of the *p*-CA-transferase, OsAT10, may reduce the amount of feruloyl-CoA available for modification of matrix polysaccharide. The absence of an effect on lignin composition or content makes the

later hypothesis less likely, since the pool of lignin precursors is also cytoplasmic (Achnine et al., 2004). Further experiments will be needed to test these various models.

"Mitchell Clade" Acyltransferases Have Different Effects on Cell Wall Hydroxycinnamoyl Esters

Both our data and that of Piston *et al.* (2010) provide genetic evidence that changing the expression of "Mitchell clade" CoA acyltransferases alters the amounts of cell wall hydroxycinnamoyl esters. Superficially, our result that *OsAt10* overexpression decreases cell wall ferulate appears to conflict with that of Piston et al. (2010), who reported that simultaneous reduced expression of *OsAt6* through *OsAt10* (i.e., construct pAFT-B) causes a ~20% reduction in the amount of FA in mature leaves. One possibility is that in *OsAT10-D1* a change in expression of other related acyltransferases causes the observed phenotype. However, that there is no measurable change in expression of related acyltransferases in *OsAT10-D1* make this model less likely (Supplemental Figure 2).

Instead, the various phenotypes observed in mutants for "Mitchell clade" members are consistent with a model in which differing OsATs have distinct functions. First, this model explains the apparent conflict between Piston et al.'s results and ours. We postulate that Piston et al. (2010) observed small or no effects because their two constructs (one simultaneously targeting *OsAt6* through *OsAt10;* and the other silencing *OsAt1*, *OsAt2*, *OsAt11*, and *OsAt12*) caused multiple small effects. Indeed, while several studies have found that BAHD acyltransferases often have promiscuous specificities (D'Auria, 2006), work with anthocyanidin-malonyl transferases (Dm3MAT1), for example, have measured discrimination for a hydroxylated substrate over a malonylated one (Unno et al., 2007). Also, PMT/OsAT4 shows at least 100-fold discrimination for *p*-coumaryl CoA over feruloyl CoA (Withers et al., 2012). Thus, it is probable that various "Mitchell clade" acyltransferases have differential affinities for the hydroxycinnamoyl-CoA adducts and candidate nucleophile acceptor molecules. This model is also consistent with the report of Withers et al. (2012) that OsAT4 (PMT) uses monolignol acceptors, rather than sugar acceptors, as the data suggest for OsAT10.

Glucose Polysaccharide, but Not Lignin, Compensation in *OsAT10-D1*

The mature cell wall of *OsAT10-D1* exhibits a ~10 to 20% increase by mass and mol% in both TFA-soluble glucose, corresponding to mixed linkage glucan and amorphous cellulose, and TFA-insoluble glucose, representing crystalline cellulose (Figure 9). In contrast, chemical, mass spectrometry, and thermogravimetric assays did not detect alterations in lignin content or

composition in the *OsAT10-D1* mutant line (Table II, Figure 10, and Supplemental Figure 5). This suggests that lignin amounts are not sensitive to changes in phenylpropanoid pathway flux that may be caused by increased OsAT10 activity. The observations that FA and glucose levels change but lignin does not might be due to spatial and temporal separation of the incorporation of hydroxycinnamates into a GAX precursor and the synthesis of lignin. Generally, our results contribute to an emerging view that plants possess molecules that are able to sense and trigger responses to specific changes in cell wall composition and/or function; however, the identity of those sensors remains largely obscure (Humphrey et al., 2007; Wolf et al., 2012).

Cell Wall Hydroxycinnamoyl Esters May Contribute to Plant Reproduction

Correlative studies suggest that FA dimerization has a role in halting plant growth via inhibition of cell wall elongation and expansion (MacAdam and Grabber, 2002; Obel et al., 2002; Sasayama et al., 2011). Thus, we might have expected plants with reduced FA dimer content to either be smaller, due to decreased ability to support themselves, or be larger, due to greater expansion of cells during growth. Indeed, the progeny of a maize line with reduced ferulate esters at the seedling stage, has recently been found to increase biomass by ~8% in field trials (Jung and Phillips, 2010). However, we observed no consistent effect on vegetative growth for greenhouse-grown *OsAt10* overexpression lines (Figure 4).

OsAT10-D1 does exhibit reduced seed yields per plant by ~20% (Figure 4). This observation correlates with the difficulty of isolating homozygous knockout lines for various *OsAt* genes (e.g., *OsAt4* and *OsAt13*, Supplemental Table II and F. Piston and J. Dubcovsky personal communication). On the other hand the low ferulate maize lines did not exhibit a change in ear mass at the stage examined (Jung and Phillips, 2010). Further studies will be needed to determine if and how grass cell wall hydroxycinnamic acids act during reproduction. From a practical perspective, restoring grain yield in plants engineered to overexpress *OsAt10* would be an important consideration for development of a dual-use crop for both food and biofuel/feed purposes, but would be less crucial for dedicated fuel and feed grasses. An obvious way to accomplish this would be to use a promoter with low expression in reproductive tissues.

Heightened Saccharification of *OsAT10-D1*

An impetus for this work was to understand if a specific genetic reduction in the amount of cell wall-associated FA would improve digestibility of cell wall sugars from modified plants for biofuel and feed production. We found that the decreased amount of FA and a proportional decrease in diferulates in *OsAT10-D1* straw did indeed lead to greater sugar yields in both

enzymatic and fungal saccharification assays (Figure 11). The quantitative similarity between the improvement in cellulase-mediated digestion and cell wall glucose content (~20%) raises the caveat that the improvement in enzymatic digestibility may not be due to altered cellulose accessibility, but rather cellulose amount. On the other hand, the larger improvement in glucose yield (~40%) from incubation with the fungus, *Penicillium sp.* YT02, is consistent with improvements in the accessibility of glucose-containing polysaccharides. Compared with the simple cellulase cocktail treatment, the pretreatment and synthesis by the fungus of a suite of enzymes might have accentuated the effects of the reduced ferulate content of the mutant.

The improvement in fungal xylose release was particularly dramatic (85%) and was accompanied by a clear increase in fungal xylanase production (Figure 11). These observations are consistent with the model that the modifications in the mutants are on the xylan polymer, which is made more accessible by reduced ability to cross-link via diferulates and ethers to lignin. We do not expect that there is a major improvement in the quality of the xylan of the *OsAT10-D1* that permits higher xylanase activity due to a reduction in FA substitution (Gilbert et al., 2008). In fact, the xylan in the mutant has a ~50% higher total hydroxycinnamoyl esters substitution rate compared with the wild type (Figure 7).

Conclusion

We find that altered expression of members of a grass-diverged and -expanded clade of BAHD acyl-CoA acyltransferases alters the amounts of hydroxycinnamic acids in grass cell walls. In particular, increased expression of *OsAt10* increases *p*-CA content but decreases FA content of rice matrix polysaccharide, consistent with our tentative assignment of this enzyme as a *p*-coumaroyl-CoA transferase. Together with the recent report that OsAT4 has *p*-CA monolignol transferase activity, this suggests that other members of the “Mitchell clade” of acyl-CoA acyltransferases likely possess feruloyl transferase activity(-ies). This insight opens the possibility of a detailed examination of the biological functions of and selective basis for acylation of the different grass cell wall polymers with hydroxycinnamates. Of practical importance toward improving the efficiency of biofuel production from grass biomass and the nutritional value of forage grasses, we have found that the increased *OsAt10* expression increases straw glucose content and improves *in vitro* digestibility. The fact that this is an overexpression effect will facilitate rapid testing of this gene in other grass species.

MATERIALS AND METHODS

Acyltransferase Identification and Phylogenetic Analysis

To identify putative BAHD acyltransferases, we downloaded the hidden Markov model profile for PF02458 from the Pfam database and then searched the annotated protein sequences of diverse plant genomes to identify potential domains using HMMER v3.0 (Finn et al., 2011). We used the following genome annotation sources and versions, which were current at the time of the analysis: *Arabidopsis thaliana*, TAIR v10; *Brachypodium dostachyon*, Phytozome v7.0; *Glycine max*, Phytozome v7.0; *Medicago truncatula*, Mt3.5; *Oryza sativa*, MSU v6.1; *Physcomitrella patens*, Phytozome v7.0; *Populus trichocarpa*, Phytozome v7.0; *Sorghum bicolor*, Phytozome v7.0; *Selaginella moellendorffii*, Phytozome v7.0. To serve as a reference for phylogenetic analysis, we downloaded the sequences of 46 previously characterized BAHD enzymes from NCBI, and identified their conserved PF02458 domains as described above. We refer to these proteins as the D'Auria set (D'Auria, 2006). In addition, we randomly selected an out-group of three PF02458-containing proteins from fungi. All phylogenetic analyses were conducted only with the Pfam domain protein sequences. Multiple segments identified by HMMER3 with similarity to the PF02458 domain for a single protein were concatenated. Redundant sequences from alternative splice versions of a single locus were removed from subsequent analyses if the domain sequence was unchanged by the splicing event. We determined the BAHD clade of each predicted protein via comparison to the D'Auria set. To do this, we used Clustal2 (Larkin et al., 2007) with default settings to build an alignment of the D'Auria set followed by limited manual adjustments with BioEdit. We used this alignment as a profile for alignment of each species' predicted BAHD enzymes. Based on these alignments, we omitted sequences that lack the region immediately surrounding the highly conserved active-site motif, HXXXD, or include an extra amino acid between them. Lack of conservation of the H was permitted, due to variation in this residue in a biochemically characterized BAHD (Walker et al., 2002).

Phylogenetic analysis was conducted in two stages. The first stage was a coarse analysis of all the BAHDs from each species relying on neighbor-joining algorithms and the second consisted of a more robust Bayesian analysis. For the first stage, the goals were to identify proteins most closely related to the "Mitchell clade" for second stage analysis and to analyze their context relative to other BAHDs. For the first stage, we used MEGA5.05 (Tamura et al., 2011) to infer and visualize neighbor-joining phylogenetic trees for each species' BAHD proteins in conjunction with the D'Auria set and the out-group sequences. Parameters were: amino acid substitutions according to the Jones-Taylor-Thorton model, gamma distribution of mutation rate among sites, distribution shape parameter of one, and gaps treated by pair-wise

deletion. Five hundred bootstraps were used to identify a consensus tree for each species. In these trees, the previously delineated BAHD clades unfailingly grouped together (D'Auria, 2006). From the phylogenetic tree made of the rice BAHDs and the D'Aruia set, we identified proteins from the D'Auria set most closely related to the "Mitchell clade." These proteins are included in Supplemental Figure 1 and consist of the taxol biosynthesis genes and the BanAAT. We used these characterized proteins as markers to identify the "Mitchell clade" and related proteins from each of the species-specific trees for further analysis of the relationships among "Mitchell clade" members from diverse species.

For the second stage of the analysis, we analyzed the relationships among BAHDs closely related to the "Mitchell clade." Selected proteins from the diverse plant species were aligned and the alignments manually edited. To generate Figure 1B we used MrBayes3.1.2 (Huelsenbeck and Ronquist, 2001) with the WAG model for amino acid substitutions and a gamma rate distribution with some invariable residues. Analysis with a subset of the data showed that this was the most probable fixed rate model for the data set. We ran the Markov Chain Monte Carlo simulation for 125,000 generations until the average standard deviation of split frequencies stabilized below 0.01. The mutli-species tree in Supplemental Figure 1 was with the same parameters run for 1.5 $X10^6$ generations.

Plant Lines and Growth Conditions

We selected mutant lines for the target genes from RiceGE, the rice mutant flanking sequence database (An et al., 2005; Jeong et al., 2006). The initial screen was conducted on the segregating progeny of the primary transgenics. Seeds from the stock center were sterilized with a 40% commercial bleach solution and germinated on a half-strength Murashige and Skoog (MS) medium containing 1.5% sucrose, 0.55 mM myo-inositol and 0.2% phytagel at 28°C with continuous white light. After seven days, the seedlings were transplanted into topsoil and grown in a greenhouse (20-30°C, 60 to 80% relative humidity). Natural day lengths <14 hours were supplemented with artificial lighting. Fertilizer (14-14-14 Slow Release) was applied every six weeks.

For genotyping, 10-20 mg leaf samples from 14-20 segregating progeny were harvested, frozen in liquid nitrogen, and ground with a Qiagen Tissuelyser (17 Hz, 1 minute). The samples were vortexed in 200 µL DNA extraction buffer containing 100 mM Tris-HCl (pH 9.5), 1 M KCl, and 10 mM EDTA (pH 8.0), incubated at 65°C for 30 min, diluted with 1 mL of H_2O, and centrifuged for 10 min at the maximum speed. The supernatant was used as the template for genotyping by PCR, with conditions as follows: 94°C, 5 min; 35 cycles of 95°C for 35 sec, 56°C

for 45 sec, and 72°C for 45 sec; concluding with 72°C for 5 minutes. Genotyping primers are listed in Supplemental Table S1. Three primers were used for each mutant line. Two primers recognized genomic sequences flanking the T-DNA insert, and one recognized a sequence near one of the T-DNA borders. Depending on the number of bands amplified, we were able to clearly distinguish heterozygous and homozygous plants. We further characterized the next two generations in selfed progeny of homozygous mutant and wild-type segregant plants of line 4A-03423, referred to herein as *OsAT10-D1*. Homozygous plants in subsequent generations were confirmed by spot-checking the genotype with PCR, and other molecular analyses, as described. Specifically, we characterized mutant progeny of 4A-03423.5, 4A-03423.12, and 4A-03423.12.9 and wild-type segregant progeny of 4A-03423.5 and 4A-03423.5.6. In this notation, the period indicates each new generation and the numbers following the period indicate the parent plant of the analyzed progeny.

Generation of *Ubi$_{pro}$:OsAt10* lines

We amplified a 1541 base pair fragment encoding *OsAt10* (*LOC_Os06g39390.1*) including both the start and stop codons from Nipponbare seedling cDNA with the cloning primers listed in Supplemental Table I. The PCR fragment was gel purified, cloned into pENTR-DTOPO (Invitrogen), and confirmed by sequencing. We then recombined the gene into the final pCAMBIA1300-Ubi-GW-Nos construct (Park et al., 2010). This binary vector contains a Gateway cassette, flanked by the maize *Ubi1* promoter and the 3´-terminator of nopaline synthase from *Agrobacterium tumefaciens*, and the *Hpt2* gene, which confers resistance to hygromycin. We used *Argrobacterium tumefaciens* EHA105 to transform fresh calli from the rice *japonica* cultivar, *Kitaake*, as previously described (Cheng et al., 1997). After regeneration of plantlets, plants were transferred to the greenhouse under conditions described above, and genotyped with primers for *Hpt2* (Supplemental Table I).

Quantitative RT-PCR

We measured gene expression in young leaf samples. The samples were harvested five weeks after transplanting to the greenhouse and consisted of the top, recently emerged or greater-than two-thirds emerged leaf of the second or third tiller. We attempted to choose morphologically and developmentally similar leaves for analysis, based on leaf length and degree of emergence/expansion. Leaves were split vertically down the mid-vein and one half dried for hydroxycinnamic acid analysis, as described below. The other half was frozen in liquid nitrogen, ground to a powder, and the RNA extracted with 1 mL of Trizol reagent (Invitrogen,

Grand Island, NY) with subsequent processing according to the manufacturer protocol. The resulting total RNA was then purified by digestion with DNaseI and cleaned up on a Nucleospin RNA II column (Macherey-Nagel, Bethlehem, PA) according to the manufacturer protocol. RNA quality was checked on a 1.4% agarose gel after denaturation with glyoxal reagent (Ambion). We synthesized cDNA from 1 µg of total RNA with VILO-Superscript (Invitrogen).

We used quantitative real time PCR to measure the expression of each target gene and potential off targets. Using an established procedure for identifying control primers (Vandesompele et al., 2002), we screened primers for three highly expressed rice genes (*Ubq5*, *eEf1α*, and *18S rRNA* ; Jain et al., 2006) and two moderately expressed genes (*Abp* and *Cc55*; Jain, 2009) for stability of expression across a set of cDNAs made from 28 rice, aerial vegetative samples collected throughout development (Supplemental Table I, LEB and PCR unpublished). Based on geNORM analysis, we used primers for *Ubq5* and *Cc55,* the two most stably expressed genes for our samples, for internal controls in the qPCR reactions. Reactions were run in a Bio-Rad CFX96 thermocycler, using SsoFAST EvaGreen Mastermix (Bio-Rad, Hercules, CA). Reaction efficiencies were calculated with LinRegPCR, which calculates the average efficiency for each primer pair based on all the reactions using those primers per plate (Ruijter et al., 2009). Efficiency-adjusted gene expression was normalized with the geometric mean of the control primers (Vandesompele et al., 2002), using the following equation: $SQRT(E_{Cc55}^{Cq(Cc55)} \times E_{Ubq5}^{Cq(Ubq5)})/E_{goi}^{Cq(goi)}$, where E and Cq indicate the average reaction efficiency and cycle number at which the threshold fluorescence level was exceeded for the designated genes, respectively, and *goi* indicates the experimental “gene-of-interest”.

Cell Wall Analyses

Preparation of Alcohol Insoluble Residue (AIR)

Due to the significant changes in cell wall content across development, we took care to harvest developmentally similar plant organs and parts for comparisons between wild-type and mutant plants in all experiments. Samples harvested for the initial screen were dried at 65°C and samples from subsequent generations at 45°C for 72 hrs. Immature tissue was ground by two rounds of shaking with a tissue homogenizer in 2 mL polypropylene tubes at 1200 rpm with two stainless steel balls for 90 sec each. Mature aerial tissue was milled with a Wiley Mill with a 5 mm screen followed by an Udy mill with a 1 mm screen. Ground tissue (5 to 500 mg) was treated with 95% ethanol (1:4 w/v) at 100°C for 30 min. After the treatment, the supernatant was removed by centrifugation (10,000 g, 10 min) and the residue was subsequently washed three to five times with 70% ethanol and dried at ~35°C under vacuum using a centrivap. The dried

powder obtained after 70% ethanol wash is designated as alcohol insoluble residue (AIR). The AIR was destarched as described by Obro et al. (2004). AIR was treated with amylase (Termamyl, Novozymes, Bagsværd, Denmark) at a loading of 0.3 U/10 mg biomass in 3-(N-morpholino) propanesulfonic acid (MOPS) buffer (50 mM, pH 7.0) at 85°C for 1 h followed by amyloglucosidase (0.33 U/10 mg biomass) and pullulanase (0.04 U/10 mg biomass) in acetate buffer, 200 mM, pH 4.5 for 2 h at 50°C. Amyloglucosidase and pullulanase were purchased from Megazyme (Bray, Ireland). The reactions were stopped by adding 3 volumes of cold 95% ethanol, vortexed, and centrifuged at 10,000 X g for 10 min. The residue obtained after centrifugation was washed three times with 70% ethanol and dried at 32°C using a CentriVap Vacuum Concentrator (Labconco, Kansas City, MO).

Analysis of Hydroxycinnamic Acids

To release esterified hydroxycinnamic acids from the cell wall, AIR (1 to 10 mg, depending on the experiment, typically 3 mg) was saponified with 500 µl of 2 N NaOH for 24 h at 25°C with mixing at 300 rpm, similar to previous descriptions (Rautengarten et al., 2012). For analysis of later generations, we doped reactions with an extraction standard, trans-cinnamic acid, but this improvement had not yet been developed for the initial screening. After saponification, the supernatant was acidified to pH < 2 with 100 µL concentrated HCl, vortexed, and extracted three times with 300 µL ethyl acetate. The extracts were combined and evaporated to dryness using a CentriVap at 32°C. The samples were dissolved in 50% (v/v) methanol prior to HPLC analysis. Care was taken to shield the samples from light during the entire process of extraction to prevent the isomerization of hydroxycinnamates in light.

Quantification of hydroxycinnamic acids was carried out on a Dionex Ultimate 3000 high performance liquid chromatography (HPLC) system (Thermo Scientific-Dionex, Sunnyvale, CA) with UV detection. Samples were separated on a reverse-phase C18 column (Synergy 4u Fusion-RP 80 Å, 250 x 2 mm, Phenomenex, Torrance, CA) with a flow of 0.3 ml/min and a gradient of solvent A (0.2%, v/v, TFA) and solvent B (acetonitrile) as follows: 0-5 min, 10% B isocratic; 5-25 min, 10-30% B linear; 25-40 min, 30% B isocratic; 40-45 min, 30-35% B linear; 45-46 min, 35-100% B linear; 46-51 min, 100% B isocratic; 51-53 min 100-10% B linear; 53-60 min 10% B isocratic. The column temperature was maintained at 30°C and detection was carried out at 320 nm. Drs. J. Ralph and F. Lu provided the ferulate dehydrodimers, which were treated with 2 N NaOH prior to running as standards (Ralph et al., 1994). To confirm that the species with corresponding retention times were diferulates, we also collected the two major dimer peaks from the HPLC and verified their mass by LC-MS.

Hydroxycinnamate Fractionation

To determine whether the changes in hydroxycinnamate content were associated with the matrix polysaccharide or the lignin fractions, 6 mg of destarched AIR were mixed with 600 uL of either 0.05 M trifluoroacetate (TFA) or water similar to a previously described method (Saulnier et al., 1995). Samples were incubated with shaking at 100 °C for up to 690 minutes. At each time point, a fraction of the sample was removed and frozen. Thawed samples were treated with 2 N NaOH for 24 hrs at 25 °C followed by neutralization with concentrated HCl. *trans*-Cinnamic acid was doped into the samples prior to three extractions with 300 uL of ethyl acetate. Combined extracts were dried with a CentriVap without heat and resuspended in 50:50 MeOH for HPLC analysis. The multiple time points show that the reaction that liberates the matrix polysaccharide goes approximately to completion. Longer times or higher acid concentrations caused degradation of the hydroxycinnamates.

High Performance Liquid Chromatography-Electrospray Ionization-Mass Spectrometry

HPLC separation of the supernatant of 5 mg samples treated for 4 hrs with 50 mM trifluoroacetate was performed using an Agilent 1290 (Santa Clara, CA) HPLC system equipped with a Phenomenex (Torrance, CA) Kinetex reversed phase column (ODS-18, 100 mm x 2.1 mm, 2.6 µm particle size). Mobile phase A consisted of 5% HPLC-grade acetonitrile (Fisher Scientific, Pittsburg, PA) and 0.1% formic acid in HPLC-grade submicron filtered water (Fisher Scientific, Pittsburg, PA). Mobile phase B consisted of 0.1% formic acid in 100% HPLC-grade acetonitrile. These mobile phase solutions were filtered and vacuum-degassed prior to use. A binary gradient at 0.3 mL/min flow rate was applied as follows: 90% solvent A and 10% solvent B from 0 to 4 min, linear gradient to 30% solvent B from 4 to 8 min, linear gradient to 50% solvent B from 8 to 9 min, 50% solvent B from 9 to 12 min, linear gradient from 12 to 13 min to 100% solvent B, 100% solvent B from 13 to 15 min, and linear gradient to return the mobile phase to 90% solvent A and 10% solvent B from 15 to 16 min, which was maintained for an additional 5 min before the next sample was injected. The HPLC column eluent was introduced into an Agilent 6538 UHD Accurate Mass QTOF (Santa Clara, CA) equipped with an electrospray ionization source operated in negative ion mode. Nitrogen was used as a nebulizing gas (40 psi) and a drying gas (325°C and 10 L/min flow rate). Fragmentor, skimmer, and capillary voltages were 160V, 65V, and 750V, respectively, and the capillary voltage was 3500V. Data was collected with Mass Hunter Acquisition (B.04.00, 2011) and analyzed with Mass Hunter Qualitative (B.04.00, 2011).

Monosaccharide composition by HPAEC

Destarched AIR (2-5 mg) was treated with 2 M TFA at 120°C for 1 h. Next the hydrolysate was dried using a CentriVap at 32°C. Monosaccharides produced by TFA hydrolysis were then redissolved in nanopure water and analyzed by high-performance anion exchange chromatography (HPAEC) with pulsed amperometric detection on an Dionex ICS-3000 system equipped with an electrochemical detector and a 4 × 250 mm CarboPac PA20 column (ØBro et al., 2004). The monosaccharides used as the external standards were obtained from Sigma-Aldrich (St. Louis, MO) and Alfa Aesar (Ward Hill, MA).

Lignin Quantification using Acetyl Bromide

Lignin was quantified via acetylbromide solubilization (Fukushima and Hatfield, 2004), followed by quantification in a 96-well plate. Briefly, AIR (5 mg) was saponified in 2 N NaOH at 25 °C for 24 h, then the supernatant was removed and the pellet incubated with 300 µL of freshly prepared acetyl bromide (25% v/v in acetic acid, Alfa Aesar, Ward Hill, MA) in screw-cap eppendorf tubes (VWR# 16466-044) at 50°C for 3 hrs in a thermomixer at 1050 rpm, with vortexing every 15 min for the last hour. After centrifuging, 100 µL of the solution was transferred to a fresh tube, followed by addition of 400 µL of 2 N NaOH and 70 µL of freshly prepared 0.5 M hydroxylamine hydrochloride. Next, 57 µL of the solution was transferred to a uv-compatible 96-well plate, followed by addition of 200 µL of glacial acetic acid. Absorption was measured at 280 nm with a SynergyHT (BioTek, Winooski, VT). The lignin content in the samples was determined with an extinction coefficient of 17.75 L $g^{-1}cm^{-1}$ corresponding to average values for grass samples (Fukushima and Hatfield, 2004). Path length was determined by measuring the height of the plate.

Pyrolysis Molecular Beam Mass Spectrometry

A commercially available molecular beam mass spectrometer (MBMS) designed specifically for biomass analysis was used for pyrolysis vapor analysis (Skyes et al., 2010). Approximately 4 mg of air-dried 20-mesh biomass was introduced into the quartz pyrolysis reactor via 80 µL deactivated stainless steel Eco-Cups provided with the autosampler. Mass spectral data from m/z 30-450 were acquired on a Merlin Automation data system version 3.0 using 17 eV electron impact ionization. Lignin estimates and S:G ratios were determined by summing the intensities of peaks assigned to lignin compounds as described (Skyes et al., 2010). Several lignin peaks were omitted in the syringyl or guaiacyl summations due to

individual peaks having associations with both S and G precursors (Evans and Milne, 1987). Note that for interpreting the ions, the “tails” of phenylpropanoid molecules are typically absent in these spectra due to MS fragmentation.

Thermogravimetric Analysis

Thermogravimetric experiments were run using a Netzsch STA 449 F3 TG-DTA instrument. Approximately 50 mg of ground sample was weighed and loaded into the thermal analyzer. Measurements were conducted in 50 mL/min gas flow. The gas was initially He; and the temperature was held at 35°C for 15 minutes and then increased to 800°C at 10 K/min. The samples were then cooled to 140°C and the gas flow was switched to 60% air in He. The samples were then again heated to 800°C at 5 K/min and then cooled to 290°C and the gas flow was switched back to He. The weight data reported in Supplemental Figure 5B were corrected for variations in water content by normalizing to the weight at 177°C, 30 minutes into the experiment.

Enzymatic Saccharification Assay

AIR (2-5 mg) was pretreated by shaking at 30°C in 500 µL of 100 mM Citrate buffer (pH 5.0) followed by incubation at 100°C for 1 hour. After cooling on the bench, final dilutions of 1:2000 NS50013, which contains a cellulase cocktail, and 1:10,000 NS50010, which contains ß-glucosidase, from the Novozymes Biomass Kit (Franklinton, NC) were added to the slurry. Reactions were incubated at 50°C with shaking with periodic removal of samples, which were stopped by freezing. Released reducing sugars were quantified by 3,5-dinitrosalicilate (DNS) assay (Ghose, 1987).

Fungal Deconstruction and Enzymatic Assays

Pretreatment of Rice Straw. Prior to pre-treatment, wild-type and mutant rice straw were soaked in 1.2% H_2SO_4 overnight. Steam-based pretreatment was performed by loading the samples into an autoclave gun and treating them at 191°C with a residence time of 2 min. Pretreated materials were then released by rapid depressurization to allow the material to explode. The pre-treated materials were collected, filtered, washed with distilled water, and stored at 4°C for subsequent degradation experiments using a modified Hägglund’s method (Hägglund, 1951).

Rice Straw Degradation. Pretreated wild-type and mutant rice straw was supplemented with 100 mL of Mandel’s media in 500-mL flasks (Mandels et al., 1970). Spores from *Penicillium*

sp. YT02 were collected from agar plates with a 0.9% NaCl solution, then adjusted to a concentration of 5.0×10^{12} spores mL^{-1}, and used as inoculum [10% (v/v)] for fungal degradation.

Protein Content. Fungal growth was estimated by the protein content in the supernatant. Mid-log fungal cell culture suspension was collected by centrifugation (14,000 x g) for 20 min at room temperature. The supernatant was collected and protein content was determined via the Bradford method.

Enzymatic Activities. Total cellulase activity was determined against Whatman no.1 filter paper (Sigma–Aldrich, St. Louis, MO) using the DNS method (Xiao et al., 2004). Total endoglucanase activity was determined with carboxymethylcellulose (CMC) (Claeyssens and Aerts, 1992) followed by reducing sugar measurements with DNS (Ghose, 1987). β-glucosidase activity was determined with *p*-nitrophenyl-β-d-glucoside and the liberation of *p*-nitrophenol was accompanied by absorption spectroscopy at 410 nm (Ghose, 1987). Xylanase activity was assayed as described elsewhere (Gessesse and Gashe, 1997). One international unit (IU) was defined as the enzymatic activity needed for the release of 1 mmol of sugar equivalents per unit volume per minute. To improve accuracy, activity values are expressed relative to the protein concentration in the media (IU/mg).

Saccharides. Fungal cultures were centrifuged and the supernatants analyzed for saccharide content by HPLC using an Aminex HPX-87H (Bio-Rad, Hercules, CA) organic acid column at 65°C. The mobile phase was 5 mM sulfuric acid at a flow rate of 0.5 mL/min. A refractive index detector was used.

Statistical Analysis.

Two-tailed Student's t-tests were used to calculate the significance of differences in cell wall and growth parameters. Homoscedastic tests were used unless the difference between the variances of the two samples was greater than 3-fold, in which case a heteroscedastic test was used.

ACKNOWLEDGEMENTS

We thank Drs. J. Harholt, M. Bowman, and Z. He for technical advice; Elias Marvinney, Carolina Peña, and Bryan Andrews for technical assistance; Drs. J. Ralph and F. Lu for providing diferulates for use as standards; Dr. Y. Wu, S. Makaju, and S. Williams for assistance with sample milling; and Drs. F. Piston and J. Dubcovsky for access to data prior to publication.

Literature Cited

Achnine L, Blancaflor EB, Rasmussen S, Dixon RA (2004) Colocalization of L-phenylalanine ammonia-lyase and cinnamate 4-hydroxylase for metabolic channeling in phenylpropanoid biosynthesis. Plant Cell **16:** 3098-3109

Agblevor FA, Evans RJ, Johnson KD (1994) Molecular-beam mass-spectrometric analysis of lignocellulosic materials : I. Herbaceous biomass. J Anal Appl Pyrolysis **30:** 125-144

Allerdings E, Ralph J, Schatz PF, Gniechwitz D, Steinhart H, Bunzel M (2005) Isolation and structural identification of diarabinosyl 8-O-4-dehydrodiferulate from maize bran insoluble fibre. Phytochemistry **66:** 113-124

An G, Lee S, Kim SH, Kim SR (2005) Molecular genetics using T-DNA in rice. Plant Cell Physiol **46:** 14-22

Banks JA, Nishiyama T, Hasebe M, Bowman JL, Gribskov M, dePamphilis C, Albert VA, Aono N, Aoyama T, Ambrose BA, Ashton NW, Axtell MJ, Barker E, Barker MS, Bennetzen JL, Bonawitz ND, Chapple C, Cheng C, Correa LGG, Dacre M, DeBarry J, Dreyer I, Elias M, Engstrom EM, Estelle M, Feng L, Finet C, Floyd SK, Frommer WB, Fujita T, Gramzow L, Gutensohn M, Harholt J, Hattori M, Heyl A, Hirai T, Hiwatashi Y, Ishikawa M, Iwata M, Karol KG, Koehler B, Kolukisaoglu U, Kubo M, Kurata T, Lalonde S, Li K, Li Y, Litt A, Lyons E, Manning G, Maruyama T, Michael TP, Mikami K, Miyazaki S, Morinaga Si, Murata T, Mueller‐Roeber B, Nelson DR, Obara M, Oguri Y, Olmstead RG, Onodera N, Petersen BL, Pils B, Prigge M, Rensing SA, Riaño-Pachón DM, Roberts AW, Sato Y, Scheller HV, Schulz B, Schulz C, Shakirov EV, Shibagaki N, Shinohara N, Shippen DE, Sørensen I, Sotooka R, Sugimoto N, Sugita M, Sumikawa N, Tanurdzic M, Theißen G, Ulvskov P, Wakazuki S, Weng JK, Willats WWGT, Wipf D, Wolf PG, Yang L, Zimmer AD, Zhu Q, Mitros T, Hellsten U, Loqué D, Otillar R, Salamov A, Schmutz J, Shapiro H, Lindquist E, Lucas S, Rokhsar D, Grigoriev IV (2011) The Selaginella Genome Identifies Genetic Changes Associated with the Evolution of Vascular Plants. Science **332:** 960-963

Beekwilder J, Alvarez-Huerta M, Neef E, Verstappen FW, Bouwmeester HJ, Aharoni A (2004) Functional characterization of enzymes forming volatile esters from strawberry and banana. Plant Physiol **135:** 1865-1878

Buanafina MMdO (2009) Feruloylation in Grasses: Current and Future Perspectives. Mol Plant **2:** 861-872

Bunzel M, Heuermann B, Kim H, Ralph J (2008) Peroxidase-catalyzed oligomerization of ferulic acid esters. J Agric Food Chem **56:** 10368-10375

Bunzel M, Ralph J, Lu F, Hatfield RD, Steinhart H (2004) Lignins and ferulate-coniferyl alcohol cross-coupling products in cereal grains. J Agric Food Chem **52:** 6496-6502

Burhenne K, Kristensen BK, Rasmussen SK (2003) A new class of N-hydroxycinnamoyltransferases. Purification, cloning, and expression of a barley agmatine coumaroyltransferase (EC 2.3.1.64). J Biol Chem **278:** 13919-13927

Carpita NC (1996) Structure and biogenesis of the cell walls of grasses. Annu Rev Plant Physiol Plant Mol Biol **47:** 445-476

Casler MD, Jung H-JG (2006) Relationships of fibre, lignin, and phenolics to in vitro fibre digestibility in three perennial grasses. Anim Feed Sci Tech **125:** 151-161

Cheng X, Sardana R, Altosaar I (1997) Rice transformation by Agrobacterium infection. *In* C Cunningham, AJR Porter, eds, Methods in Biotechnology: Recombinant Proteins from Plants -- Production and Isolation of Clinically Useful Compounds, Vol 3. Humana, Totowa, NJ, pp 1-9

Claeyssens M, Aerts G (1992) Characterisation of cellulolytic activities in commercial Trichoderma reesei preparations: An approach using small, chromogenic substrates. Bioresour Technol **39:** 143-146

D'Auria JC (2006) Acyltransferases in plants: a good time to be BAHD. Curr Opin Plant Biol **9:** 331-340
Dudareva N, Pichersky E (2000) Biochemical and molecular genetic aspects of floral scents. Plant Physiol **122:** 627-634
Evans RJ, Milne TA (1987) Molecular characterization of the pyrolysis of biomass. Energy & Fuels **1:** 123-137
Fanta GF, Abbott TP, Herman AI, Burr RC, Doane WM (1984) Hydrolysis of wheat straw hemicellulose with trifluoroacetic acid. Fermentation of xylose with Pachysolen tannophilus. Biotechnol Bioeng **26:** 1122-1125
Faulds CB, Mandalari G, LoCurto R, Bisignano G, Waldron KW (2004) Arabinoxylan and mono- and dimeric ferulic acid release from brewer's grain and wheat bran by feruloyl esterases and glycosyl hydrolases from Humicola insolens. Appl Microbiol Biotechnol **64:** 644-650
Fincher GB (2009) Revolutionary times in our understanding of cell wall biosynthesis and remodeling in the grasses. Plant Physiol **149:** 27-37
Finn RD, Clements J, Eddy SR (2011) HMMER web server: interactive sequence similarity searching. Nucleic Acids Res **39:** W29-37
Fukushima RS, Hatfield RD (2004) Comparison of the acetyl bromide spectrophotometric method with other analytical lignin methods for determining lignin concentration in forage samples. J Agric Food Chem **52:** 3713-3720
Gessesse A, Gashe BA (1997) Production of alkaline xylanase by an alkaliphilic Bacillus sp. isolated from an alkaline soda lake. J of Appl Microbiol **83:** 402-406
Ghose TK (1987) Measurement of Cellulase Activities. Pure Appl Chem **59:** 257-268
Gilbert HJ, Stålbrand H, Brumer H (2008) How the walls come crumbling down: recent structural biochemistry of plant polysaccharide degradation. Current Opinion in Plant Biology **11:** 338-348
Grabber JH, Hatfield RD, Ralph J (1998) Diferulate cross-links impede the enzymatic degradation of non-lignified maize walls. J Sci Food Agric **77:** 193-200
Grabber JH, Quideau S, Ralph J (1996) p-Coumaroylated syringyl units in maize lignin: Implications for [beta]-ether cleavage by thioacidolysis. Phytochemistry **43:** 1189-1194
Grabber JH, Ralph J, Hatfield RD (1998) Ferulate cross-links limit the enzymatic degradation of synthetically lignified primary walls of maize. J Agric Food Chem **46:** 2609-2614
Hägglund E (1951). *In* E Hägglund, ed, Chemistry of Wood. Academic, New York, NY, pp 374-379
Hatfield R, Marita J, Frost K, Grabber J, Ralph J, Lu F, Kim H (2009) Grass lignin acylation: p-coumaroyl transferase activity and cell wall characteristics of C3 and C4 grasses. Planta **229:** 1253-1267
He X, Zhang J (2005) Rapid subfunctionalization accompanied by prolonged and substantial neofunctionalization in duplicate gene evolution. Genetics **169:** 1157-1164
Hoffmann L, Maury Sp, Martz Fß, Geoffroy P, Legrand M (2003) Purification, cloning, and properties of an acyltransferase controlling shikimate and quinate ester intermediates in phenylpropanoid metabolism. J Biol Chem **278:** 95-103
Huelsenbeck JP, Ronquist F (2001) MRBAYES: Bayesian inference of phylogenetic trees. Bioinformatics **17:** 754-755
Humphrey TV, Bonetta DT, Goring DR (2007) Sentinels at the wall: cell wall receptors and sensors. New Phytol **176:** 7-21
Ishii T (1991) Isolation and characterization of a diferuloyl arabinoxylan hexasaccharide from bamboo shoot cell-walls. Carbohydr Res **219:** 15-22
Ishii T, Hiroi T, Thomas JR (1990) Feruloylated xyloglucan and *p*-coumaroyl arabinoxylan oligosaccharides from bamboo shoot cell-walls. Phytochemistry **29:** 1999-2003

Jain M (2009) Genome-wide identification of novel internal control genes for normalization of gene expression during various stages of development in rice. Plant Science **176:** 702-706

Jain M, Nijhawan A, Tyagi AK, Khurana JP (2006) Validation of housekeeping genes as internal control for studying gene expression in rice by quantitative real-time PCR. Biochem Biophys Res Commun **345:** 646-651

Jeong DH, An S, Park S, Kang HG, Park GG, Kim SR, Sim J, Kim YO, Kim MK, Kim J, Shin M, Jung M, An G (2006) Generation of a flanking sequence-tag database for activation-tagging lines in japonica rice. Plant J **45:** 123-132

Jung HG, Phillips RL (2010) Putative seedling ferulate ester (sfe) maize mutant: Morphology, biomass yield, and stover cell wall composition and rumen degradability. Crop Sci. **50:** 403-418

Jung KH, An G, Ronald PC (2008) Towards a better bowl of rice: assigning function to tens of thousands of rice genes. Nat Rev Genet **9:** 91-101

Kellogg EA (2001) Evolutionary History of the Grasses. Plant Physiol. **125:** 1198-1205

Kosma DK, Molina I, Ohlrogge JB, Pollard M (2012) Identification of an Arabidopsis fatty alcohol:caffeoyl-Coenzyme A acyltransferase required for the synthesis of alkyl hydroxycinnamates in root waxes. Plant Physiol **160:** 237-248

Kovacs K, Macrelli S, Szakacs G, Zacchi G (2009) Enzymatic hydrolysis of steam-pretreated lignocellulosic materials with Trichoderma atroviride enzymes produced in-house. Biotechnol Biofuels **2:** 14

Lal R (2005) World crop residues production and implications of its use as a biofuel. Environ Int **31:** 575-584

Lam TB-T, Iiyama K, Stone BA (2003) Hot alkali-labile linkages in the walls of the forage grass Phalaris aquatica and Lolium perenne and their relation to in vitro wall digestibility. Phytochemistry **64:** 603-607

Lanoue A, Burlat V, Henkes GJ, Koch I, Schurr U, Rose US (2009) De novo biosynthesis of defense root exudates in response to Fusarium attack in barley. New Phytol

Larkin MA, Blackshields G, Brown NP, Chenna R, McGettigan PA, McWilliam H, Valentin F, Wallace IM, Wilm A, Lopez R, Thompson JD, Gibson TJ, Higgins DG (2007) Clustal W and Clustal X version 2.0. Bioinformatics **23:** 2947-2948

Luo J, Fuell C, Parr A, Hill L, Bailey P, Elliott K, Fairhurst SA, Martin C, Michael AJ (2009) A novel polyamine acyltransferase responsible for the accumulation of spermidine conjugates in Arabidopsis seed. Plant Cell **21:** 318-333

Lynd LR, Laser MS, Bransby D, Dale BE, Davison B, Hamilton R, Himmel M, Keller M, McMillan JD, Sheehan J, Wyman CE (2008) How biotech can transform biofuels. Nat Biotechnol **26:** 169-172

MacAdam JW, Grabber JH (2002) Relationship of growth cessation with the formation of diferulate cross-links and *p*-coumaroylated lignins in tall fescue leaf blades. Planta **215:** 785-793

Mandels M, Andreotti R, Roche C (1970) Measurement of saccharifying cellulase. Biotech Bioeng Symp **6:** 21-33

Mitchell RA, Dupree P, Shewry PR (2007) A novel bioinformatics approach identifies candidate genes for the synthesis and feruloylation of arabinoxylan. Plant Physiol **144:** 43-53

Molina I, Beisson-Li Y, Beisson F, Ohlrogge JB, Pollard M (2009) Identification of an Arabidopsis feruloyl-CoA transferase required for suberin synthesis. Plant Physiol **151:** 1317-1328

Mueller-Harvey I, Hartley RD, Harris PJ, Curzon EH (1986) Linkage of *p*-coumaroyl and feruloyl groups to cell-wall polysaccharides of barley straw. Carbohyd Res **148:** 71-85

Obel N, Nuemetzler L, Pauly M (2006) Hemicelluloses and cell expansion. *In* J-P Verbelen, K Vissenberg, eds, Plant Cell Monographs: The Expanding Cell, Vol 5. Springer, Berlin, pp 57-88

Obel N, Porchia AC, Scheller HV (2002) Dynamic changes in cell wall polysaccharides during wheat seedling development. Phytochemistry **60:** 603-610

Obel N, Porchia AC, Scheller HV (2003) Intracellular feruloylation of arabinoxylan in wheat: evidence for feruloyl-glucose as precursor. Planta **216:** 620-629

ØBro J, Harholt J, Scheller HV, Orfila C (2004) Rhamnogalacturonan I in Solanum tuberosum tubers contains complex arabinogalactan structures. Phytochemistry **65:** 1429-1438

Oikawa A, Lund CH, Sakuragi Y, Scheller HV (2012) Golgi-localized enzyme complexes for plant cell wall biosynthesis. Trends Plant Sci

CJ, Bart R, Chern M, Canlas PE, Bai W, Ronald PC (2010) Overexpression of the endoplasmic reticulum chaperone BiP3 regulates XA21-mediated innate immunity in rice. PLoS ONE **5:** e9262

Pendall E, Osanai YUI, Williams AL, Hovenden MJ (2011) Soil carbon storage under simulated climate change is mediated by plant functional type. Global Change Biology **17:** 505-514

Piston F, Uauy C, Fu L, Langston J, Labavitch J, Dubcovsky J (2010) Down-regulation of four putative arabinoxylan feruloyl transferase genes from family PF02458 reduces ester-linked ferulate content in rice cell walls. Planta **231:** 677-691

Ralph J (2010) Hydroxycinnamates in lignification. Phytochem Rev **9:** 65-83

Ralph J, Quideau S, Grabber JH, Hatfield RD (1994) Identification and synthesis of new ferulic acid dehydrodimers present in grass cell walls. J Chem Soc, Perkin Trans 1**:** 3485-3498

Rautengarten C, Ebert B, Herter T, Petzold CJ, Ishii T, Mukhopadhyay A, Usadel B, Scheller HV (2011) The interconversion of UDP-arabinopyranose and UDP-arabinofuranose is indispensable for plant development in Arabidopsis. Plant Cell **23:** 1373-1390

Rautengarten C, Ebert B, Ouellet M, Nafisi M, Baidoo EE, Benke P, Stranne M, Mukhopadhyay A, Keasling JD, Sakuragi Y, Scheller HV (2012) Arabidopsis Deficient in Cutin Ferulate encodes a transferase required for feruloylation of omega-hydroxy fatty acids in cutin polyester. Plant Physiol **158:** 654-665

Richardson A, Wojciechowski T, Franke R, Schreiber L, Kerstiens G, Jarvis M, Fricke W (2007) Cuticular permeance in relation to wax and cutin development along the growing barley (*Hordeum vulgare*) leaf. Planta **225:** 1471-1481

Ruijter JM, Ramakers C, Hoogaars WM, Karlen Y, Bakker O, van den Hoff MJ, Moorman AF (2009) Amplification efficiency: linking baseline and bias in the analysis of quantitative PCR data. Nucleic Acids Res **37:** e45

Santiago R, Reid LM, Arnason JT, Zhu X, Martinez N, Malvar RA (2007) Phenolics in maize genotypes differing in susceptibility to Gibberella Stalk Rot (*Fusarium graminearum* Schwabe). J Agric Food Chem **55:** 5186-5193

Santiago R, Sandoya G, Butrón A, Barros J, Malvar RA (2008) Changes in phenolic concentrations during recurrent selection for resistance to the mediterranean corn borer (*Sesamia nonagrioides* Lef.). J Agric Food Chem **56:** 8017-8022

Sasayama D, Azuma T, Itoh K (2011) Involvement of cell wall-bound phenolic acids in decrease in cell wall susceptibility to expansins during the cessation of rapid growth in internodes of floating rice. J Plant Physiol **168:** 121-127

Saulnier L, Vigouroux J, Thibault JF (1995) Isolation and partial characterization of feruloylated oligosaccharides from maize bran. Carbohydr Res **272:** 241-253

Scheller HV, Ulvskov P (2010) Hemicelluloses. Annu Rev Plant Biol **61:** 263-289

Schreiber L (2010) Transport barriers made of cutin, suberin and associated waxes. Trends in Plant Science **15:** 546-553

Skyes R, Yung M, Novaes E, Kirst M, Peter G, Davis M (2010) High-throughput screening of plant cell-Wall composition using pyrolysis molecular beam mass spectroscopy. *In* JR Mielenz, ed, Biofuels: Methods and Protocols, Vol 581. Humana Press, pp 169-183

Takahama U, Oniki T (1994) Effects of ascorbate on the oxidation of derivatives of hydroxycinnamic acid and the mechanism of oxidation of sinapic acid by cell wall-bound peroxidases. Plant Cell Physiol **35:** 593-600

Tamura K, Peterson D, Peterson N, Stecher G, Nei M, Kumar S (2011) MEGA5: molecular evolutionary genetics analysis using maximum likelihood, evolutionary distance, and maximum parsimony methods. Mol Biol Evol **28:** 2731-2739

Tuominen L, Johnson V, Tsai C-J (2011) Differential phylogenetic expansions in BAHD acyltransferases across five angiosperm taxa and evidence of divergent expression among populus paralogues. BMC Genomics **12:** 236

Unno H, Ichimaida F, Suzuki H, Takahashi S, Tanaka Y, Saito A, Nishino T, Kusunoki M, Nakayama T (2007) Structural and mutational studies of anthocyanin malonyltransferases establish the features of BAHD enzyme catalysis. J Biol Chem **282:** 15812-15822

US-DOE (2011) U.S. Billion-Ton Update: Biomass supply for a bioenergy and bioproducts industry. RD Perlack, BJ Stokes, eds. Oak Ridge National Labs, Oak Ridge, TN, p 227

Vandesompele J, De Preter K, Pattyn F, Poppe B, Van Roy N, De Paepe A, Speleman F (2002) Accurate normalization of real-time quantitative RT-PCR data by geometric averaging of multiple internal control genes. Genome Biol **3:** RESEARCH0034

Vogel J (2008) Unique aspects of the grass cell wall. Curr Opin Plant Biol **11:** 301-307

Walker K, Long R, Croteau R (2002) The final acylation step in taxol biosynthesis: cloning of the taxoid C13-side-chain N-benzoyltransferase from Taxus. Proc Natl Acad Sci U S A **99:** 9166-9171

Withers S, Lu F, Kim H, Zhu Y, Ralph J, Wilkerson CG (2012) Identification of grass-specific enzyme that acylates monolignols with p-coumarate. J Biol Chem **287:** 8347-8355

Wolf S, Hematy K, Hofte H (2012) Growth control and cell wall signaling in plants. Annu Rev Plant Biol **63:** 381-407

Xiao Z, Storms R, Tsang A (2004) Microplate-based filter paper assay to measure total cellulase activity. Biotechnol Bioeng **88:** 832-837

Zhou JZ, Xue K, Xie JP, Deng Y, Wu LY, Cheng XH, Fei SF, Deng SP, He ZL, Van Nostrand JD, Luo YQ (2012) Microbial mediation of carbon-cycle feedbacks to climate warming. Nat Clim Change **2:** 106-110

FIGURE LEGENDS

Figure 1. (A) Structures of relevant hydroxycinnamic acids. **(B)** Inferred Bayesian phylogeny of the rice "Mitchell Clade" BAHD acyl CoA-utilizing enzymes that includes the following: the rice acyltransferases (OsAT); the Arabidopsis protein, AT3G62160, that allowed this clade to be identified by Mitchell (2007); biochemically characterized BAHD-IV and BAHD-III proteins as an outgroup, ACT and VAAT (Burhenne et al., 2003; Beekwilder et al., 2004); Arabidopsis proteins that use hydroxycinnamoyl-CoA adducts as substrates, HCT and SFT (Hoffmann et al., 2003; Molina et al., 2009); and the rice genes that cluster with the Arabidopsis HCT (HCT-like). Proteins are identified by the locus ID that encodes them or their Genbank ID, as well proposed names. Clade credibility values are 100 unless shown. The two major subclades are designated clade i and ii. Color intensity of the circles on the tree branches indicates the level of RNA expression in terms of counts of Sanger ESTs and representation in massively parallel signature sequences (MPSS) data.

Figure 2. Cell wall hydroxycinnamate composition of leaf blades (left column) and leaf sheaths (right column) of T-DNA mutant rice lines. Data are for homozygous wild-type segregant plants (solid bars) and homozygous mutant plants (hashed bars). Each plant line is designated by the repository ID and the putative target gene. **(A** and **D)** Average ferulic acid content from an alcohol insoluble residue (AIR) preparation. **(B** and **E)** *p*-Coumaric acid content from AIR. **(C** and **F)** The ratio of ferulic acid (FA) to *p*-coumaric acid (*p*-CA). Side tillers from lines *1B-00523* and *2D-40243* were harvested 10-weeks after germination. All other lines were harvested 7-weeks after germination. Averages from samples from two to three plants for each genotype were measured independently. Error bars indicate standard deviation. '*' indicates significant differences at $p < 0.05$ and '**' indicates significant differences at $p < 0.01$ (Student's t-test).

Figure 3. Genomic position of the T-DNA insertion and gene expression data for *OsAT10-D1* activation tagged lines. **(A)** Representation of the rice chromosomes near the T-DNA insertion site. Exons are represented by wide bars with the direction of transcription indicated by arrows. The insertion site is represented by the triangle, with the left border, nearest the CaMV 35S transcriptional enhancer elements, represented by 'L'. cDNA regions targeted for amplification in qPCR are depicted as black bands. 'RT' stands for retrotransposon and 'hypoth.' indicates hypothetical. *OsFBK16* encodes an F-box and kelch-domain containing protein. **(B)** Average relative gene expression determined via qPCR shows that among genes within 20 kb of the insertion site only *OsAt10* expression is altered significantly in young leaves of homozygous plants with the T-DNA insertion (hashed) compared with wilde-type segregants (solid). The observed minor variations in other nearby genes were not consistent among the 3 biological replicates assayed. Error bars represent the standard deviation of 3-4 biological replicates. Genes with significantly higher expression ($p < 0.01$, Student's t-test) are marked with an asterisk.

Figure 4. *OsAT10-D1* has normal vegetative development. **(A)** *OsAT10-D1* plants (*4A-03423.5* progeny) compared with the wild-type segregants (*4A-03423.1* progeny) at senescence, 7 months after planting. **(B)** Average dry biomass at senescence. **(C)** Average seed mass per plant at senescence. Grey bars indicate wild type (WW, *4A-03423.1* progeny), and hatched bars indicate mutant (TT, *4A-03423.5* and *4A-03423.12* progeny). N = 12. Error bars represent 2*SEM. '*' indicates significant differences at $p < 0.05$ via Student's t-test.

Figure 5. *OsAT10-D1* shows alterations in cell wall hydroxycinnamic acids. Data are for a wild-type segregants lacking the insert (grey bars, progeny of *4A-03423.1*) and progeny of homozygous mutants (cross hatched bars, progeny of *4A-03423.5*; and horizontal bars, progeny

of *4A-03423.12*) for young leaves and a pool of mature straw. **(A)** Ferulic acid content. **(B)** *p*-Coumaric acid content. **(C)** The ratio of ferulic acid (FA) to *p*-coumaric acid (*p*-CA). **(D)** Ferulate dimer amounts, the ratio of FA to dimer, and the ratio of dimer to total hydroxycinnamates (HCA) for AIR from young leaf samples in A-C. Error bars are 2*SEM of 3 to 5 biological replicates for young leaves and 2*SEM of technical duplicates for mature straw. '*' indicates significance via Student's t-test at $p < 0.05$, and '**' indicates significance at $p < 0.01$, and '***' indicates significance at $p < 1 \times 10^{-6}$, which applies to both mutant samples.

Figure 6. Independent *OsAt10* overexpression plants (cross-hatch) also show altered ratios of hydroxycinnamic acids (HCA) relative to wild-type plants (solid). **(A)** qRT-PCR shows that primary transgenic *Ubi_{pro}:OsAt10* lines 4 and 5 have increased expression of *OsAt10* relative to a developmentally matched nontransgenic escape (*Kit-1 = Ubi_{pro}:OsAt10-1*). Relative expression is normalized to the average WT amount. **(B)** Hydroxycinnamic acid content in terms of ferulic acid (FA), *p*-coumaric acid (*p*-CA), and the sum of ferulic acid dimer peaks, of a young leaf from wild-type, "escape" plants and primary transgenic plants. HCA data is also shown for another developmentally matched, escape plant (*Kit-2 = Ubi_{pro}:OsAt10-2*). **(C)** FA:*p*-CA ratio and FA:dimer ratio. '*' indicates significance via Student's t-test at $p < 0.05$.

Figure 7. The cell wall alteration in *OsAT10-D1* hydroxcinnamates is predominantly in the TFA-soluble fraction. Data are for mature straw from wild type (solid, *4A-03423.5* progeny) and mutant (hatched, *4A-03423.1* progeny). P indicates the pellet and S the supernatant after trifluoroacetate treatment (TFA) or water treatment (no TFA). The numbers indicate the minutes of TFA treatment. **(A)** Ferulic acid content in AIR. **(B)** *p*-Coumaric acid content in AIR. **(C)** The ratio of ferulic acid to *p*-coumaric acid. '*' indicates significance via Student's t-test at $p < 0.05$ and '**' indicates significance at $p < 0.01$.

Figure 8. The modified hydroxycinnamates in *OsAT10-D1* are esterified to a five-carbon sugar. **(A)** Liquid chromatography-mass spectrometry shows the total ion abundances in the ethyl acetate extracts for (a) wild type and (b) mutant after 50 mM trifluoroacetate (TFA) and 2 M NaOH and (c) wild type and (d) mutant after 50 mM TFA treatment only. Labeled peaks were consistent both with standards, when available, and with their masses. *trans*-Cinnamate was added as an extraction control. **(B and C)** Electrospray ionization (ESI) mass spectra from total ion chromatograms. "M" denotes the major ion and the other masses visible in B & C are as labeled. These compounds may be present in solution, such as due to reaction with TFA, or formed by interaction with the mobile phases. Though ESI is a "soft ionization" method in which compounds are typically not fragmented, sometimes fragmentation can occur during the electrospray process if weak bonds are present. **(B)** The major ion in the mass spectrum for unknown peak 1 is consistent with a *p*-coumaroylated five-carbon sugar. **(C)** The major ion in the mass spectrum for unknown peak 2 is consistent with a feruloylated five-carbon sugar.

Figure 9. Destarched AIR from *OsAT10-D1* mature straw (hatched*, 4A-03423.5* progeny) has increased glucose content relative to that of the wild type (solid*, 4A-03423.1* progeny). **(A)** Mass analysis shows significant increases in glucose both after trifluoroacetate (TFA) and after additional treatment with sulfuric acid (TFA->H2SO4), as well as with the sum of the two treatments. **(B)** Analysis of the molecular fraction (mol %) of monomeric sugars released by TFA in the mutant relative to the wild type shows an increase in glucose equal to the decrease in the sum of the decreases in xylose, arabinose, and other sugars. Error bars show 2*SEM of three replicates. '**' indicates a difference at $p < 0.01$ and '*' at $p < 0.05$ via Student's t-test.

Figure 10. Principal component analysis of pyrolysis-molecular beam-mass spectrometry data for *OsAT10D-1* corroborates the change in extractable phenolics, but shows no difference in

lignin composition. **(A)** First two components for technical replicates of total biomass (negative in principal component (PC) 1) and AIR (positive in PC1) for wild-type straw (WT, diamonds and squares, progeny of 4A-03423.5) and mutant straw (Mut, triangles and X's, progeny of 4A-03423.1). **(B)** Loadings plot for PC2 of (A). The mass to charge ratios of the four most differentially abundant ions are shown. The ions that are overrepresented in mutant tissue are 120 (4-vinylphenol or 2,3-dihydrobenzofuran), 91 (fragment of 2,3-dihydrobenzofuran and most phenols) and 94 (phenol). The ion that is most underrepresented in the mutant is 150 (coumaryl alcohol/coniferyl alcohol). **(C)** PCA for mutant and wild-type residue after 2 N NaOH extraction. Samples are poorly distinguished indicating that the principle components of variation are extractable and, therefore, are not polymeric lignin.

Figure 11. *OsAT10-D1* exhibits increased enzymatic and fungal deconstructability. **(A)** An enzyme cocktail of cellulase and ß-glucosidase releases more sugar from destarched AIR from mature straw of *OsAT10-D1* (red diamonds, *4A-03423.5* progeny) than from straw of the wild type (light grey circles, *4A-03423.1* progeny). AIR was pretreated at 100 degrees for one hour at pH 5.5 prior to addition of enzyme. Error bars show the values of two technical replicates. **(B)** *Penicillium sp.* YT02 releases greater amounts of sugar from rice straw of *OsAT10-D1* (diamonds, *4A-03423.5* progeny) than from wild-type straw (circles, *4A-03423.1* progeny) pretreated via acid-explosion. Grey symbols indicate glucose, red symbols xylose, and white symbols arabinose. Error bars show 2*SEM of five replicate cultures. Raw values and difference data are provided in Supplemental Table III. **(C)** Xylanase activity (dashed lines, red symbols) in the fungal-straw slurry is enhanced in the presence of the mutant straw (diamonds) relative to in the wild-type straw (circles); whereas, carboxymethyl cellulase actitvity (solid lines, grey symbols) is unchanged. IU is nmoles of sugar per minute per mL. Error bars show 2*SEM of five replicate cultures.

Supplemental Figure 1. Inferred Bayesian phylogeny for BAHD CoA acyltransferases identified from diverse species based on grouping closely with the biochemically characterized proteins that are similar to the "Mitchell clade" of BAHD proteins, namely BanAAT, and the taxol biosynthesis genes. Branch likelihood scores are >95% if not specified. Subclades i and ii, described in the text and Figure 1B, are marked. SCT and SDT are the most closely related Arabidopsis proteins for which functions have been identified (Luo et al. 2009). The note "no HCA phenotype" is based on Rautengarten et al. (2012). HCA is hydroxycinnamate.

Supplemental Figure 2. Quantitative gene expression analysis reveals no significant changes in the expression of acyltransferases related to *OsAt10* in *OsAT10-D1* (*4A-03423.5*, + insert, cross-hatched bars) and negative segregant lines (*4A-03423.1*, - insert, solid bars). Shown are the average relative expression data for each target gene and related BAHD acyltransferases in young leaves. Error bars are 2*SEM of three to four biological replicates. '*' indicates significance via Student's t-test at $p < 0.05$.

Supplemental Figure 3. *OsAT10-D1* shows consistent alterations in cell wall hydroxycinnamic acids. Data are for young leaves from a third generation of progeny of negative segregant (NS) wild-type line (*4A-03423.1.9*, grey bars) and of a mutant line homozygous for the insert (*4A-03423.5.6*, crosshatched bars). **(A)** Ferulic acid content in an alcohol insoluble residue (AIR) preparation. **(B)** *p*-Coumaric acid content from AIR. **(C)** The ratio of ferulic acid (FA) to *p*-coumaric acid (*p*-CA). The average and error bars indicate 2*SEM for the shown biological young leaf replicates. * indicates significance via Student's t-test at $p < 0.05$ and ** indicates significance at $p < 0.01$.

Supplemental Figure 4. Gene expression and hydroxycinnamate content of the second generation of *Ubi$_{pro}$:OsAt10-4* plants reveals a similar phenotype to the *OsAT10-D1* line. The wild type is shown in grey and the mutant in crosshatch. **(A)** qRT-PCR analysis of RNA isolated from flag leaf of a tiller from the 4-5 leaf stage shows increased expression of *OsAt10* in the mutant relative to the wild type. **(B)** Hydroxycinnamic acids (HCA), i.e., ferulic acid (FA), *p*-coumaric acid (*p*-CA), released from AIR from mature straw from wild-type and mutant plants by saponification. N = 3 for the wild type and N = 7 for the mutant. Error bars indicate 2*SEM for the average of the replicates. '*' indicates significance via Student's t-test at $p < 0.05$ and '**' indicates significance at $p < 0.01$.

Supplemental Figure 5. Destarched AIR from OsAT10-D1 mature straw has increased glucose (Glc) content relative to that of the wild type, but no other significant changes by mass in xylose (Xyl), arabinose (Ara), galactose (Gal), fucose (Fuc), rhammnose (Rha), galacturonic acid (GalA), or glucuronic acid (GlcA). Wild-type (*4A-03423.1* progeny) samples are solid and mutant (*4A-03423.5* progeny) samples are hatched. Error bars show 2*SEM of three replicates. '*' indicates a significant difference at $p < 0.05$ via Student's t-test.

Supplemental Figure 6. Thermogravimetric analysis detects no mass difference upon heating between wild-type and mutant mature straw. **(A)** Example gravimetric traces throughout heating. The first heating phase (red line, right axis) represents heating in the absence of oxygen and the second represents heating in the presence of oxygen (combustion). Data are normalized to values at 30 min (177°C), which represent the initial dry weights. **(B)** Selected times report on biomass composition. WT and *OsAT10-D1* are indistinguishable in terms of the mass of char (blue bars) remaining after pyrolysis at 800°C (blue bars, t = 112 min), the ash content after combustion (red bars, t = 250 min), and, by extension, the fraction of the char that is combustible (yellow bars, difference between char and ash). Switchgrass, oak, and duckweed samples are shown for comparison. Values are the % of the dry weight. When error bars are shown, values are averages and the error bars are 2*SEM of 2-4 technical replicates.

Supplemental Figure 7. Enzymatic activity in media during *Penicillium sp.* YT02 incubation with straw from the wild type (circles) and *OsAT10-D1* (diamonds). FPA (dashed lines) is the activity on cellulose filter paper. ß-glucosidase activity (solid lines) uses cellobiose as a substrate. IU is nmoles of sugar per minute per mL. Data are normalized for mg of total protein. Error bars show 2*SEM of five replicate cultures.

Table I. BAHD acyl-CoA transferases encoded in selected sequenced plant genomes.

Species	# putative BAHD proteins: Total (# Perfect HXXXD)[a]	Clade V: Total (# Perfect HXXXD) [a,b]	AT Clade i[c]	AT Clade ii[c]
Physcomitrella patens	17 (16)	8 (7)	0	0
Selaginella moellendorffii	74 (65)	19 (19)	0	0
Arabidopsis thaliana	64 (61)	25 (25)	1	0
Populus tricocarpa	125 (121)	25 (24)	0	0
Medicago truncatula	89 (83)	30 (27)	1	0
Glycine max	142 (135)	70 (65)	2	0
Oryza sativa	122 (117)	61 (60)	10	10
Sorghum bicolor	89 (85)	49 (48)	8	4
Brachypodium dystachion	83 (78)	38 (38)	12	4

[a] Consists of nonredundant predicted protein sequences identified via HMMER3.0 based on PFAM v. 25 and that contain the region surrounding the conserved active site motif, HXXXD, though proteins with single amino acid variations in the H are included. The number in parentheses is the number with the strict HXXXD motif. See Results for justification.
[b] Clade identified in D'Auria 2006.
[c] Acyltransferase (AT) protein clades delineated in Figure 1B and Supplemental Figure 1.

Table II. Lignin amounts and S:G ratios from AIR after 2 N NaOH extraction of greenhouse grown plants.

Line	Parental Genotype	Material	ABSL [a] (% mass)	S/G ratio [b]	Standardized Lignin [c] (% mass)
WT[d]	*4A-03423.1*	mature straw	5.5 ± 0.5	0.67 ± 0.01	5.7 ± 0.2
OsAT10-D1	*4A-03423.5*	mature straw	5.5 ± 0.5	0.75 ± 0.11	5.5 ± 0.1
OsAT10-D1	*4A-03423.12*	mature straw	5.7 ± 0.6	ND [e]	ND
WT	*4A-03423*	leaf sheath	ND	0.39 ± 0.05	5.9 ± 0.1
OsAT10-D1	*4A-03423*	leaf sheath	ND	0.36 ± 0.13	5.5 ± 0.7
WT	*4A-03423*	leaf blade	ND	0.52 ± 0.13	3.4 ± 0.1
OsAT10-D1	*4A-03423*	leaf blade	ND	0.52 ± 0.09	3.4 ± 0.3

[a] Acetylbromide soluble lignin expressed in terms of mg/mg for pools of straw, measured in triplicate, or 2 to 3 individual bioreplicates, measured in duplicate. Errors are standard deviations.
[b] Average ± standard deviation of singlicate measurements of 2 to 3 plants for the earlier generation, and two technical replicates of pools of 12 plants for the later generation samples, as determined by py-MBMS.
[c] As determined via py-MBMS and calibrated for each type of rice sample (i.e., straw, leaf, sheath) based on ABSL data for a larger set of rice samples.
[d] negative segregant, wild type.
[e] ND = not determined

Supplemental Table I. Sequence of primers used for genotyping and gene expression in this study.

See Excel file.

Supplemental Table II. Summary of the rice acyltransferase mutant screen. Primers for genotyping and gene expression analysis are listed in Supplemental Table I.

Gene Name [a]	Locus ID (LOC_) [b]	EST Count [c]	Mutant Line ID (PFG_)	cv [d]	Line Class (Insert Position)	# Plants Genotyped	Insert Detected	Gene Expression (primer position)	Immature leaf and sheath cell wall hydroxycinnamic acid phenotype [e]
OsAt1	*Os01g42880*	87	*3A-13924*	DJ	AT [f]	14	No	ND [g]	ND
OsAt2	*Os01g42870*	27	NA [h]						
OsAt3	*Os05g04584*	49	*3A-02783*	DJ	AT		No	ND	ND
OsAt4	*Os01g18744*	51	*3A-02300*	DJ	Insert/AT [i]	20	Yes, no homozygotes	ND	ND
			3A-09297	DJ	Insert/AT		No	ND	ND
OsAt5	*Os05g19910*	17	*2A-20021*	DJ	AT (~4 kb 5' of start)	20	Yes	~3000-fold increase (2nd exon)	Leaf and sheath: increase in FA:*p*-CA ratio
			1C-03624	HY	Insert [j]		No	ND	ND
OsAt6	*Os01g08380*	80	*1C-06931*	HY	Insert		No	ND	ND
			3A-08459	DJ	AT		No	ND	ND
			2D-40810	HY	AT	20	Yes	ND	None
OsAt7	*Os05g08640*	19	*2A-40095*	HY	Insert/AT (near 3' end of last exon)	19	Yes	~4-fold reduction (1st exon) ~5000-fold reduction (2nd exon)	Sheath: decrease FA
OsAt8	*Os06g39470*	6	NA						
OsAt9	*Os01g09010*	211	NA						
OsAt10	*Os06g39390*	38	*4A-03423* [k]	DJ	AT (~8.5 kb 5' of start)	16	Yes	~200-fold increase (2nd exon)	Leaf and Sheath: decrease FA, possible increase in *p*-CA[l]
OsAt11	*Os04g11810*	0	NA						
OsAt12	*Os04g09590*	0	*3A-16373*	DJ	AT	20	Yes	ND	None
			2D-41616	HY	AT	20	Yes	ND	None
OsAt13	*Os10g01930*	3	*2D-10182*	DJ	Insert/AT	20	Yes, no homozygotes	ND	ND

OsAt14	*Os10g02000*	0	NA						
OsAt15	*Os10g01920*	11	*1B-00523*	DJ	AT (~7 kb 3' of start)	20	Yes	~100-fold increase	Leaf: decrease FA
OsAt16	*Os10g01800*	0	*2D-40243*	DJ	AT		No	ND	None
OsAt17	*Os10g03360*	0	NA						
OsAt18	*Os10g03390*	2	*4A-04176*	DJ	AT	20	Yes	ND	None
OsAt19	*Os04g09260*	8	NA						
OsAt20	*Os06g48560*	0	NA						
Totals	20		17 (for 12 genes)				11 confirmed, 2 no homozyg. for insert		4 phenotypes

[a] *Oryza sativa* (Os) acyltransferase (At) gene names were assigned based on an early phylogenic analysis, that has since been revised.
[b] Annotation MSUv6.
[c] Sum of ESTs from all organs/stages from rice Sanger EST data available through 2009.
[d] DJ and HY indicate *O. sativa* var. *japonica* cv. Dongjin and cv. Hwayoung, respectively.
[e] For homozygous mutants relative to wild-type segregant siblings. CA signifies *p*-coumaric acid. FA signifies ferulic acid. A change in FA:*p*-CA ratio is only mentioned when a phenotype in neither FA nor CA alone appear to change.
[f] AT signifies a putative activation tagged line in which the T-DNA insert possesses transcription activation elements.
[g] ND signifies not determined.
[h] NA signifies that no rice activation lines were available at the inception of the study.
[i] Insert/AT signifies that the T-DNA possesses transcription activation sequences but is inserted within, or <300 base pairs away from, the gene.
[j] Insert signifies that the T-DNA is inserted within, or <300 base pairs away from, the gene.
[k] *OsAT10-D1*
[l] Variation in *p*-CA among replicates reduced the significance of the possible increase in *p*-CA in the first generation of mutants characterized.

Supplemental Table III. Average ± standard deviation of sugar composition of the media during the course of *Penicillium sp.* YT02 incubation with straw from *OsAT10-D1* (Mut) plants and the wild-type segregant (WT) plants. N = 5.

	Glucose			Xylose			Arabinose		
Time (hrs)	**WT (mg/mL)**	**Mut (mg/mL)**	**Δ %**	**WT (mg/mL)**	**Mut (mg/mL)**	**Δ %**	**WT (mg/mL)**	**Mut (mg/mL)**	**Δ %**
12	0.42 ± 0.01	0.42 ± 0.02	0	0.17 ± 0.03	0.32 ± 0.04	88	0.05 ± 0.02	0.05 ± 0.01	0
24	1.4 ± 0.1	1.5 ± 0.4	3	0.7 ± 0.3	1.4 ± 0.5	106	0.14 ± 0.05	0.24 ± 0.01	71
36	2.1 ± 0.1	2.3 ± 0.2	9	0.8 ± 0.2	1.8 ± 0.4	116	0.27 ± 0.03	0.40 ± 0.01	48
48	2.7 ± 0.1	4.4 ± 0.3	65	1.2 ± 0.5	2.3 ± 0.2	95	0.5 ± 0.2	0.39 ± 0.02	-19
60	3.5 ± 0.1	4.7 ± 0.3	35	1.7 ± 0.3	2.7 ± 0.2	64	0.6 ± 0.2	0.63 ± 0.02	5
72	3.4 ± 0.1	6.1 ± 0.2	82	1.8 ± 0.1	3.7 ± 0.4	102	0.5 ± 0.5	0.60 ± 0.03	25
84	3.3 ± 0.1	4.8 ± 0.1	47	2.0 ± 0.2	2.9 ± 0.2	45	0.6 ± 0.3	0.80 ± 0.05	35
96	1.8 ± 0.1	3.4 ± 0.2	97	1.4 ± 0.1	2.5 ± 0.2	84	0.5 ± 0.2	0.64 ± 0.03	28
120	1.1 ± 0.1	1.4 ± 0.1	28	1.6 ± 0.1	2.4 ± 0.2	48	0.5 ± 0.2	0.48 ± 0.03	7
Avg			**46**			**82**			**25**

	Galactose			Mannose			Cellobiose		
Time (hrs)	**WT (mg/mL)**	**Mut (mg/mL)**	**Δ %**	**WT (mg/mL)**	**Mut (mg/mL)**	**Δ %**	**WT (mg/mL)**	**Mut (mg/mL)**	**Δ %**
12	0.02 ± 0.01	0.02 ± 0.01	0	0.04 ± 0.01	0.04 ± 0.01	0	0.20 ± 0.01	0.09 ± 0.01	-55
24	0.11 ± 0.02	0.04 ± 0.01	-62	0.18 ± 0.02	0.16 ± 0.01	-9	0.38 ± 0.01	0.36 ± 0.02	-4
36	0.09 ± 0.03	0.10 ± 0.01	11	0.14 ± 0.06	0.20 ± 0.03	48	0.54 ± 0.01	0.35 ± 0.02	-35
48	0.18 ± 0.06	0.16 ± 0.01	-13	0.42 ± 0.04	0.23 ± 0.04	-44	0.70 ± 0.01	0.55 ± 0.04	-22
60	0.15 ± 0.02	0.27 ± 0.03	80	0.38 ± 0.03	0.45 ± 0.03	20	0.85 ± 0.02	0.81 ± 0.05	-5
72	0.16 ± 0.04	0.12 ± 0.02	-25	0.24 ± 0.04	0.48 ± 0.02	100	0.95 ± 0.01	1.2 ± 0.2	27
84	0.15 ± 0.02	0.40 ± 0.03	170	0.15 ± 0.03	0.30 ± 0.02	103	0.73 ± 0.03	0.80 ± 0.05	10
96	0.65 ± 0.01	0.24 ± 0.01	-63	0.10 ± 0.02	0.40 ± 0.02	300	0.60 ± 0.02	0.80 ± 0.04	34
120	0.36 ± 0.01	0.03 ± 0.02	-17	0.36 ± 0.05	0.30 ± 0.01	-17	0.37 ± 0.03	0.78 ± 0.02	110
Avg			**10**			**63**			**14**

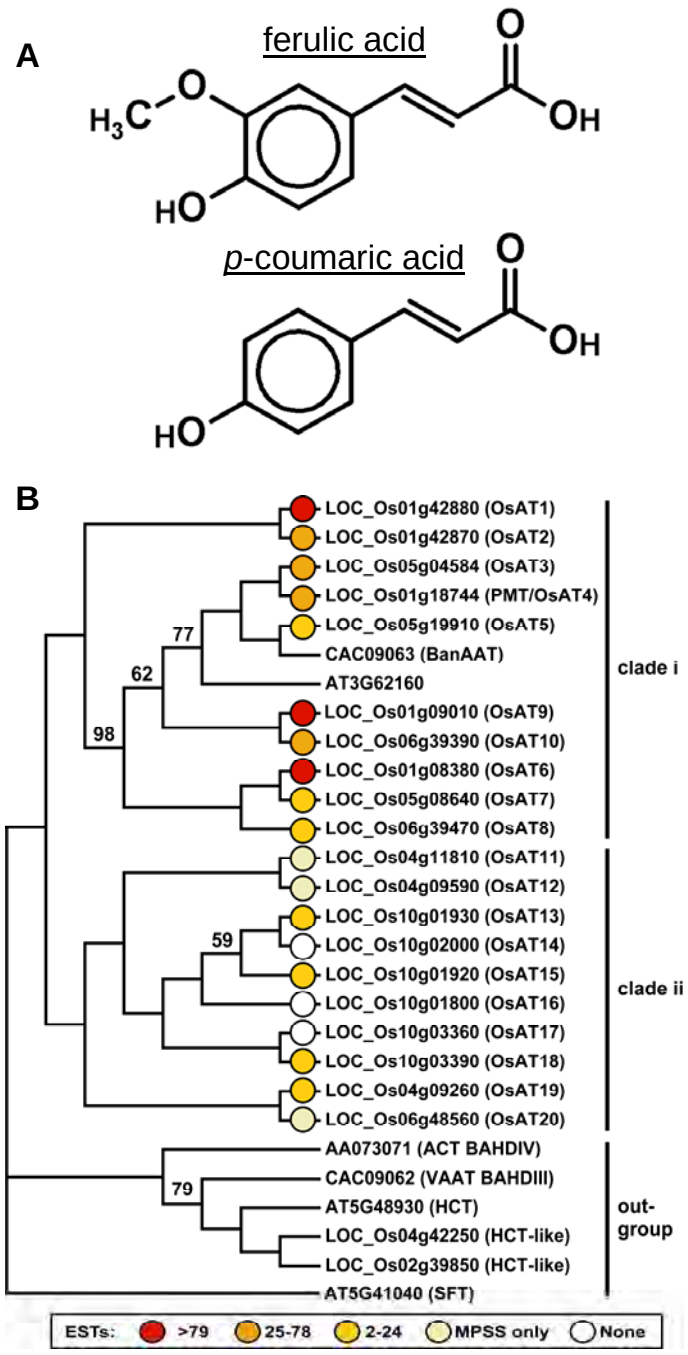

Figure 1. (A) Structures of relevant hydroxycinnamic acids. **(B)** Inferred Bayesian phylogeny of the rice "Mitchell Clade" BAHD acyl CoA-utilizing enzymes that includes the following: the rice acyltransferases (OsAT); the Arabidopsis protein, AT3G62160, that allowed this clade to be identified by Mitchell (2007); biochemically characterized BAHD-IV and BAHD-III proteins as an outgroup, ACT and VAAT (Burhenne et al., 2003; Beekwilder et al., 2004)); Arabidopsis proteins that use hydroxycinnamoyl-CoA adducts as substrates, HCT and SFT (Hoffmann et al., 2003; Molina et al., 2009); and the rice genes that cluster with the Arabidopsis HCT (HCT-like). Proteins are identified by the locus ID that encodes them or their Genbank ID, as well proposed names. Clade credibility values are 100 unless shown. The two major subclades are designated clade i and ii. Color intensity of the circles on the tree branches indicates the level of RNA expression in terms of counts of Sanger ESTs and representation in massively parallel signature sequences (MPSS) data.

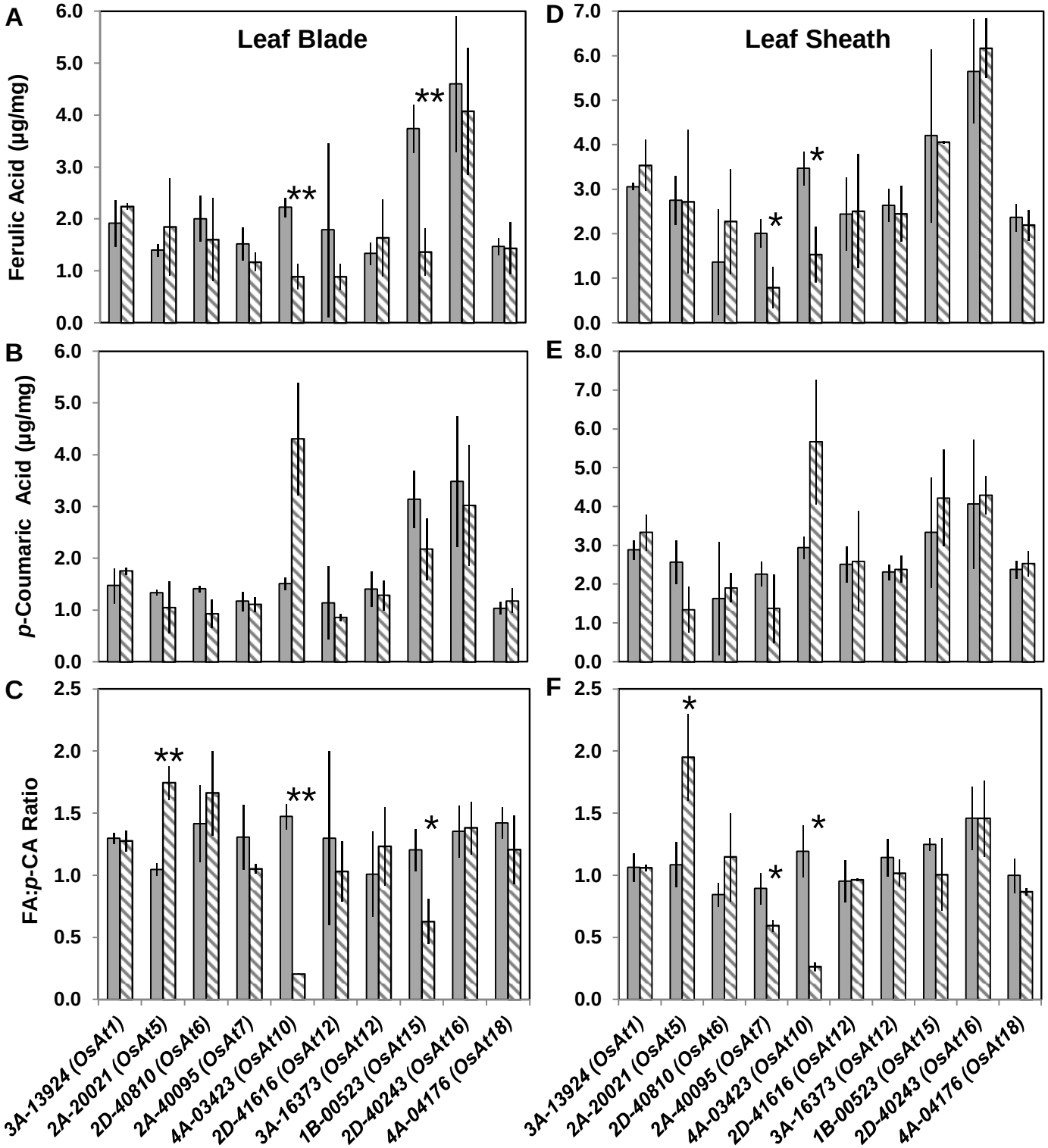

Figure 2. Cell wall hydroxycinnamate composition of leaf blades (left column) and leaf sheaths (right column) of T-DNA mutant rice lines. Data are for homozygous negative segregant plants (solid bars) and homozygous mutant plants (hashed bars). Each plant line is designated by the repository ID and the putative target gene. **(A** and **D)** Average ferulic acid content from an alcohol insoluble residue (AIR) preparation. **(B** and **E)** *p*-Coumaric acid content from AIR. **(C** and **F)** The ratio of ferulic acid (FA) to *p*-coumaric acid (*p*-CA). Side tillers from lines *1B-00523* and *2D-40243* were harvested 11-weeks after germination. All other lines were harvested 7-weeks after germination. Error bars indicate standard deviation. Samples from two to three plants for each genotype were measured independently. '*' indicates significant differences at $p < 0.05$ and '**' indicates significant differences at $p < 0.01$ (Student's t-test).

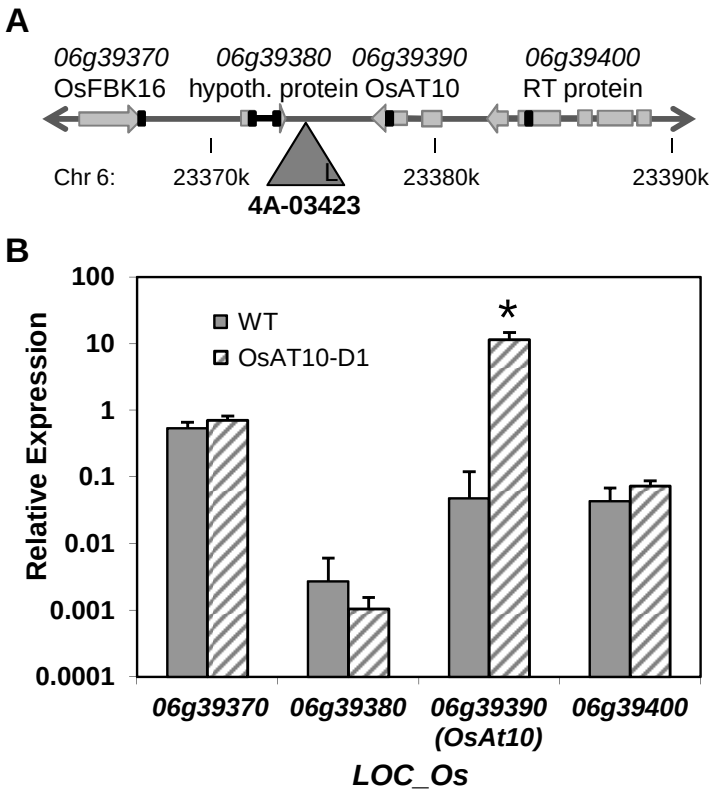

Figure 3. Genomic position of the T-DNA insertion and gene expression data for *OsAT10-D1* activation tagged lines. **(A)** Representation of the rice chromosomes near the T-DNA insertion site. Exons are represented by wide bars with the direction of transcription indicated by arrows. The insertion site is represented by the triangle, with the left border, nearest the CaMV 35S transcriptional enhancer elements, represented by 'L'. cDNA regions targeted for amplification in qPCR are depicted as black bands. 'RT' stands for retrotransposon and 'hypoth.' indicates hypothetical. *OsFBK16* encodes an F-box and kelch-domain containing protein. **(B)** Average relative gene expression determined via qPCR shows that among genes within 20 kb of the insertion site only *OsAt10* expression is altered significantly in young leaves of homozygous plants with the T-DNA insertion (hashed) compared with negative segregants (solid). The observed minor variations in other nearby genes were not consistent among the 3 biological replicates assayed. Error bars represent the standard deviation of 3-4 biological replicates. Genes with significantly higher expression ($p < 0.01$, Student's t-test) are marked with an asterisk.

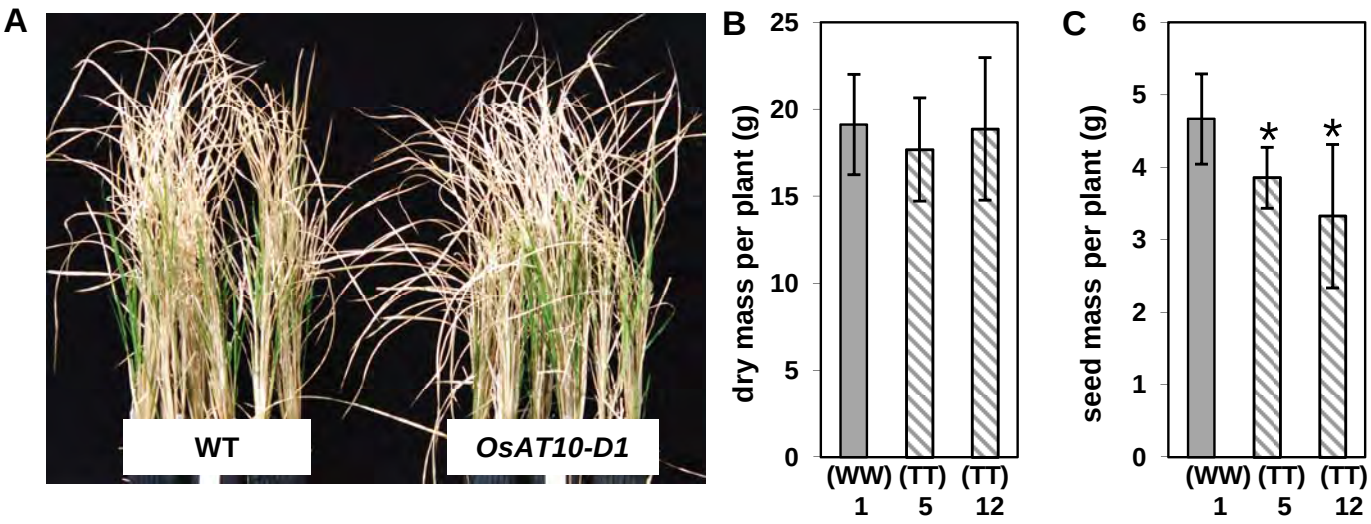

Figure 4. *OsAT10-D1* has normal vegetative development. **(A)** *OsAT10-D1* plants (*4A-03423.5* progeny) compared with the wild-type segregants (*4A-03423.1* progeny) at senescence, 7 months after planting. **(B)** Dry biomass at senescence. **(C)** Seed mass at senescence. Grey bars indicate wild type (WW, *4A-03423.1* progeny), and hatched bars indicate mutant (TT, *4A-03423.5* and *4A-03423.12* progeny). N = 12. Error bars represent 2*SEM. '*' indicates significant differences at $p < 0.05$ via Student's t-test.

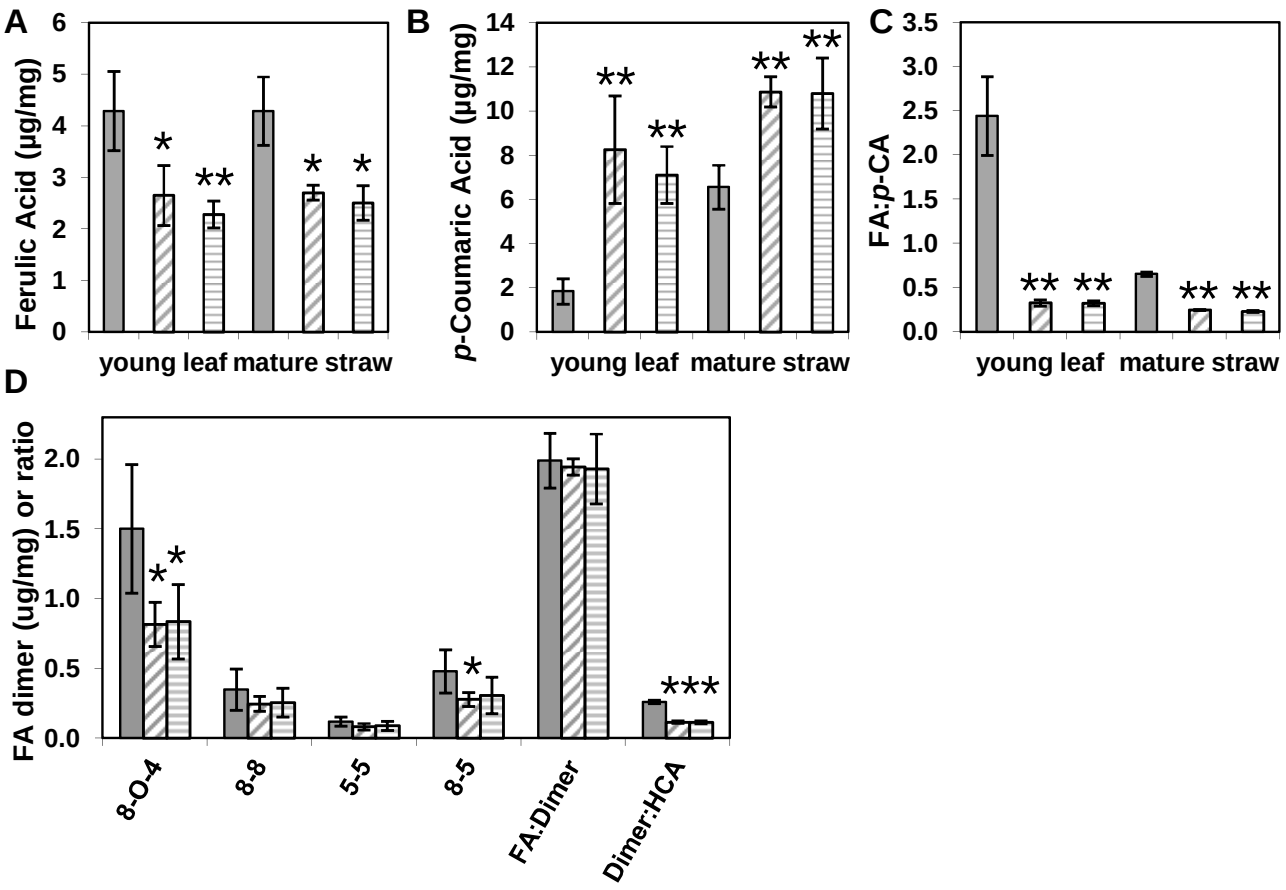

Figure 5. *OsAT10-D1* shows alterations in cell wall hydroxycinnamic acids. Data are for a wild type segregants lacking the insert (grey bars, progeny of *4A-03423.1*) and progeny of homozygous mutants (cross hatched bars, progeny of *4A-03423.5*; and horizontal bars, progeny of *4A-03423.12*) for young leaves and a pool of mature straw. **(A)** Ferulic acid content. **(B)** *p*-Coumaric acid content. **(C)** The ratio of ferulic acid (FA) to *p*-coumaric acid (*p*-CA). **(D)** Ferulate dimer amounts, the ratio of FA to dimer, and the ratio of dimer to total hydroxycinnamates (HCA) for AIR from young leaf samples in A-C. Error bars are 2*SEM of 3 to 5 biological replicates for young leaves and 3*SEM of technical replicates for mature straw. '*' indicates significance via Student's t-test at $p < 0.05$, and '**' indicates significance at $p < 0.01$, and '***' indicates significance at $p < 1 \times 10^{-6}$.

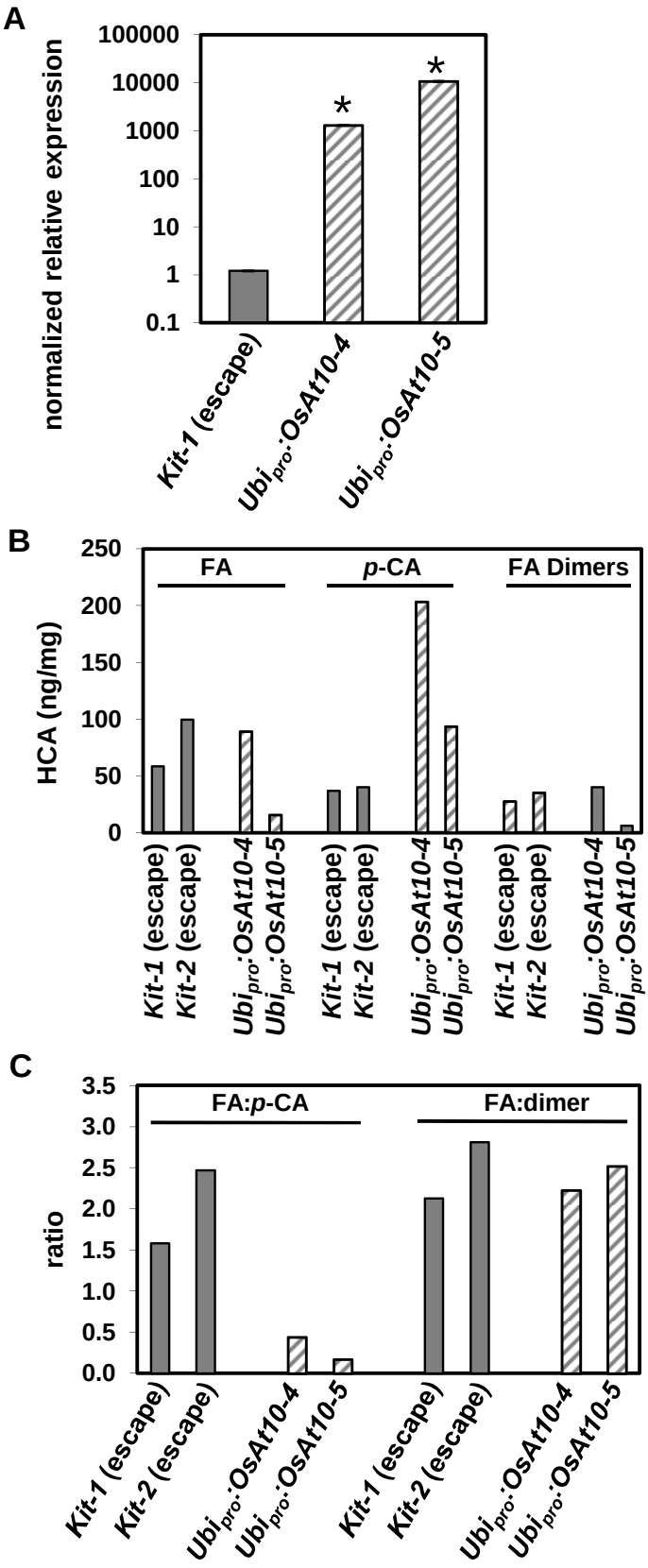

Figure 6. Independent *OsAt10* overexpression plants (cross-hatch) also show altered ratios of hydroxycinnamic acids (HCA) relative to wild-type plants (solid). **(A)** qRT-PCR shows that primary transgenic *Ubi$_{pro}$:OsAt10* lines 4 and 5 have increased expression of *OsAt10* relative to a developmentally matched nontransgenic escape (*Kit-1* = *Ubi$_{pro}$:OsAt10-1*). Relative expression is normalized to the average WT amount. **(B)** Hydroxycinnamic acid content in terms of ferulic acid (FA), *p*-coumaric acid (*p*-CA), and the sum of ferulic acid dimer peaks, of a young leaf from wild-type, "escape" plants and primary transgenic plants. HCA data is also shown for another developmentally matched, escape plant (*Kit-2* = *Ubi$_{pro}$:OsAt10-2*). **(C)** FA:*p*-CA ratio and FA:dimer ratio. '*' indicates significance via Student's t-test at $p < 0.05$.

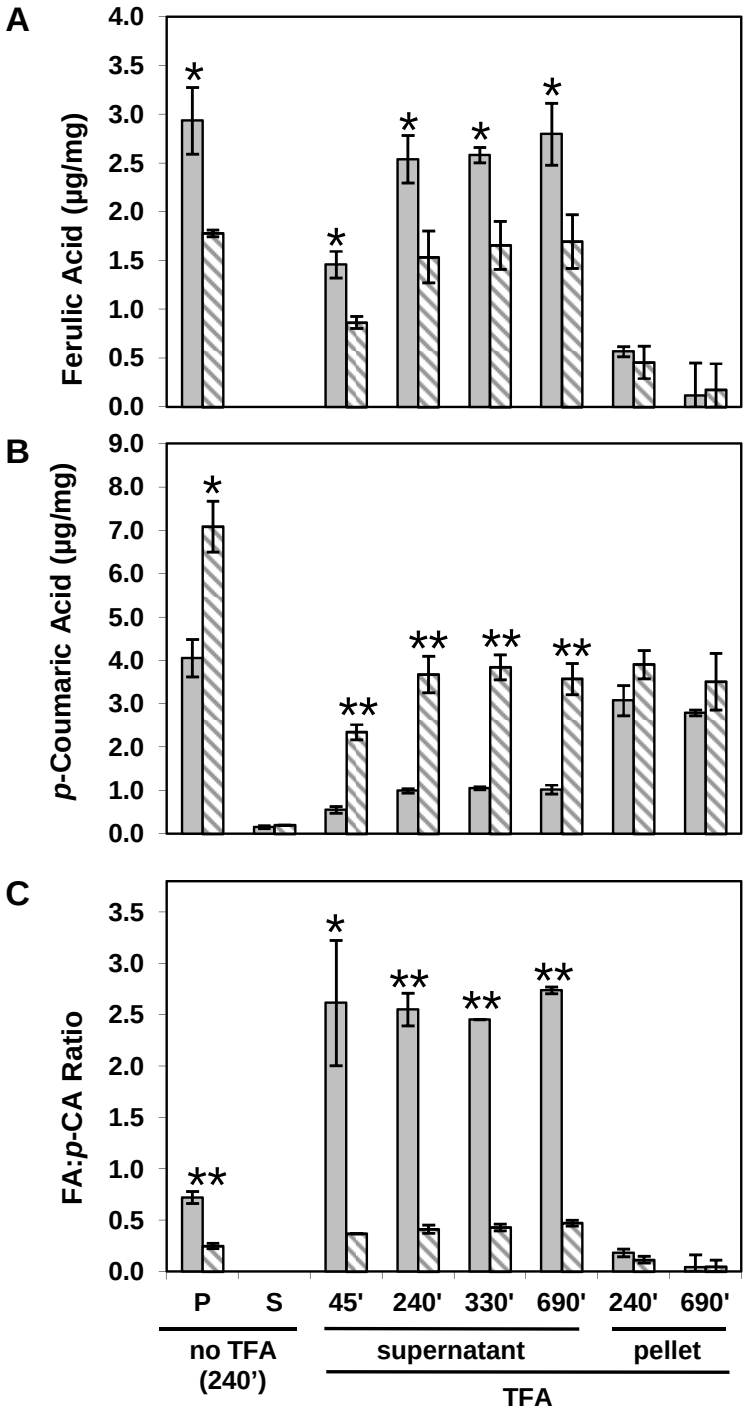

Figure 7. The cell wall alteration in *OsAT10-D1* hydroxcinnamates is predominantly in the TFA-soluble fraction. Data are for mature straw from wild type (solid, *4A-03423.5* progeny) and mutant (hatched, *4A-03423.1* progeny). P indicates the pellet and S the supernatant after trifluoroacetate treatment (TFA) or water treatment (no TFA). The numbers indicate the minutes of TFA treatment. **(A)** Ferulic acid content in AIR. **(B)** *p*-Coumaric acid content in AIR. **(C)** The ratio of ferulic acid to *p*-coumaric acid. '*' indicates significance via Student's t-test at $p < 0.05$ and '**' indicates significance at $p < 0.01$.

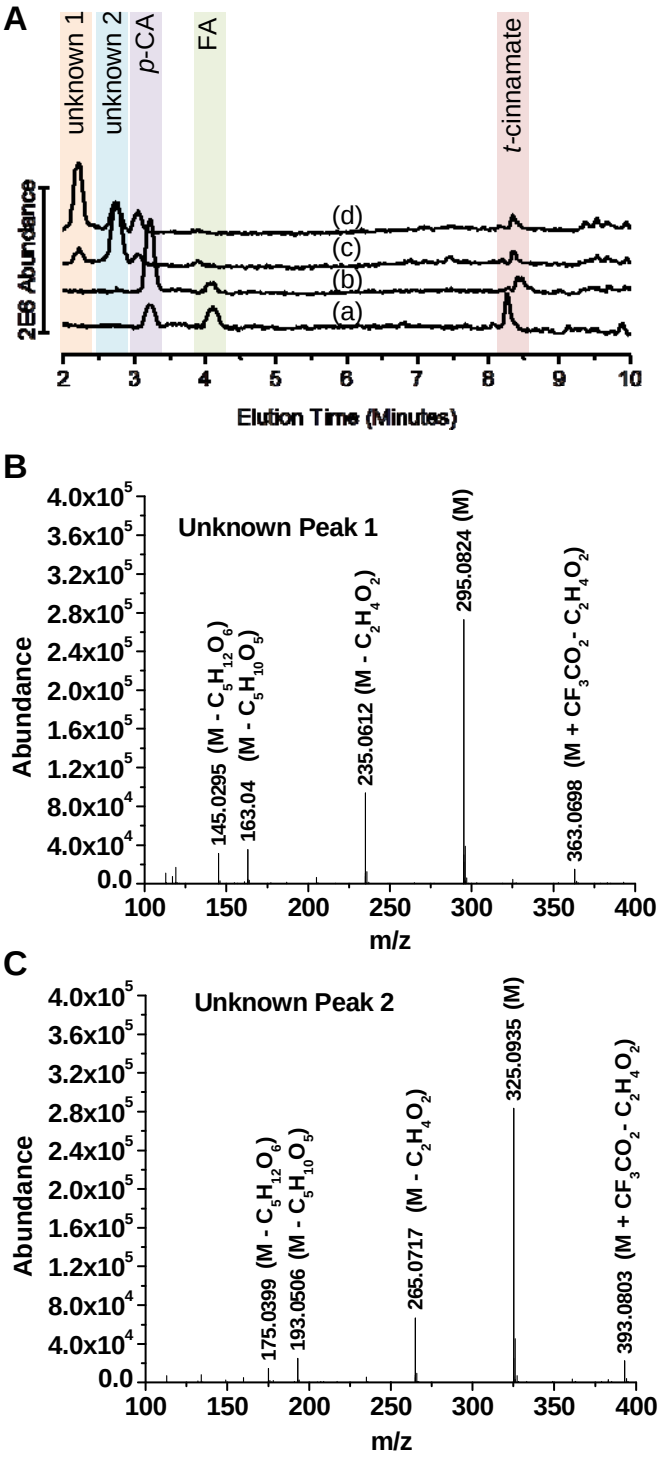

Figure 8. The modified hydroxycinnamates in *OsAT10-D1* are esterified to a five-carbon sugar. **(A)** Liquid chromatography-mass spectrometry shows the total ion abundances in the ethyl acetate extracts for (a) wild type and (b) mutant after 50 mM TFA and 2 M NaOH and (c) wild type and (d) mutant after 50 mM TFA treatment only. Labeled peaks were consistent both with standards, when available, and with mass spectra. *trans*-Cinnamate was added as an extraction control. **(B and C)** are electrospray ionization (ESI) mass spectra from a total ion chromatogram. "M" denotes the major ion and the other masses visible in B & C are as labeled. These compounds may be present in solution, such as due to reaction with TFA, or formed by interaction with the mobile phases. Though ESI is a "soft ionization" method in which compounds are typically not fragmented, sometimes fragmentation can occur during the electrospray process if weak bonds are present. **(B)** The major ion in the mass spectrum for unknown peak 1 is consistent with a *p*-coumaroylated five-carbon sugar. **(C)** The major ion in the mass spectrum for unknown peak 2 is consistent with a feruloylated five-carbon sugar.

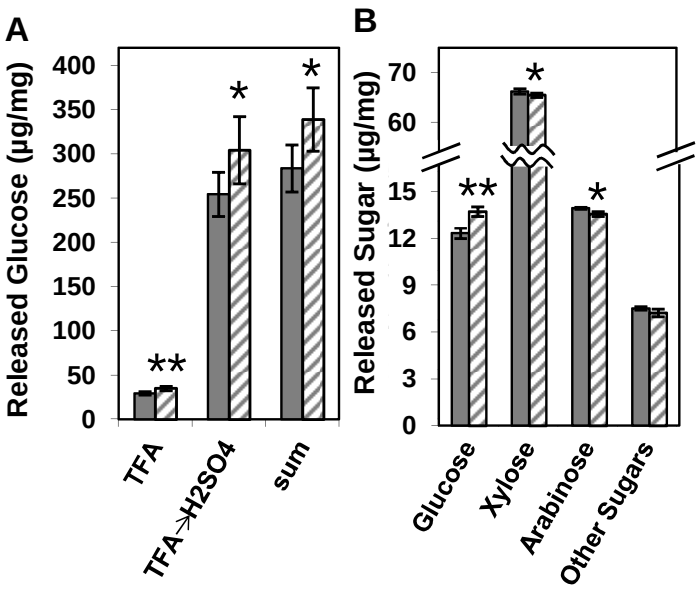

Figure 9. Destarched AIR from *OsAT10-D1* mature straw (hatched*, 4A-03423.5* progeny) has increased glucose content relative to that of the wild type (solid*, 4A-03423.1* progeny). **(A)** Mass analysis shows significant increases in glucose both after trifluoroacetate (TFA) and after additional treatment with sulfuric acid (TFA->H2SO4), as well as with the sum of the two treatments. **(B)** Analysis of the molecular fraction (mol %) of monomeric sugars released by TFA in the mutant relative to the wild type shows an increase in glucose that sums to the decreases in xylose, arabinose, and other sugars. Error bars show 2*SEM of three replicates. '**' indicates a difference at $p < 0.01$ and '*' at $p < 0.05$ via Student's t-test.

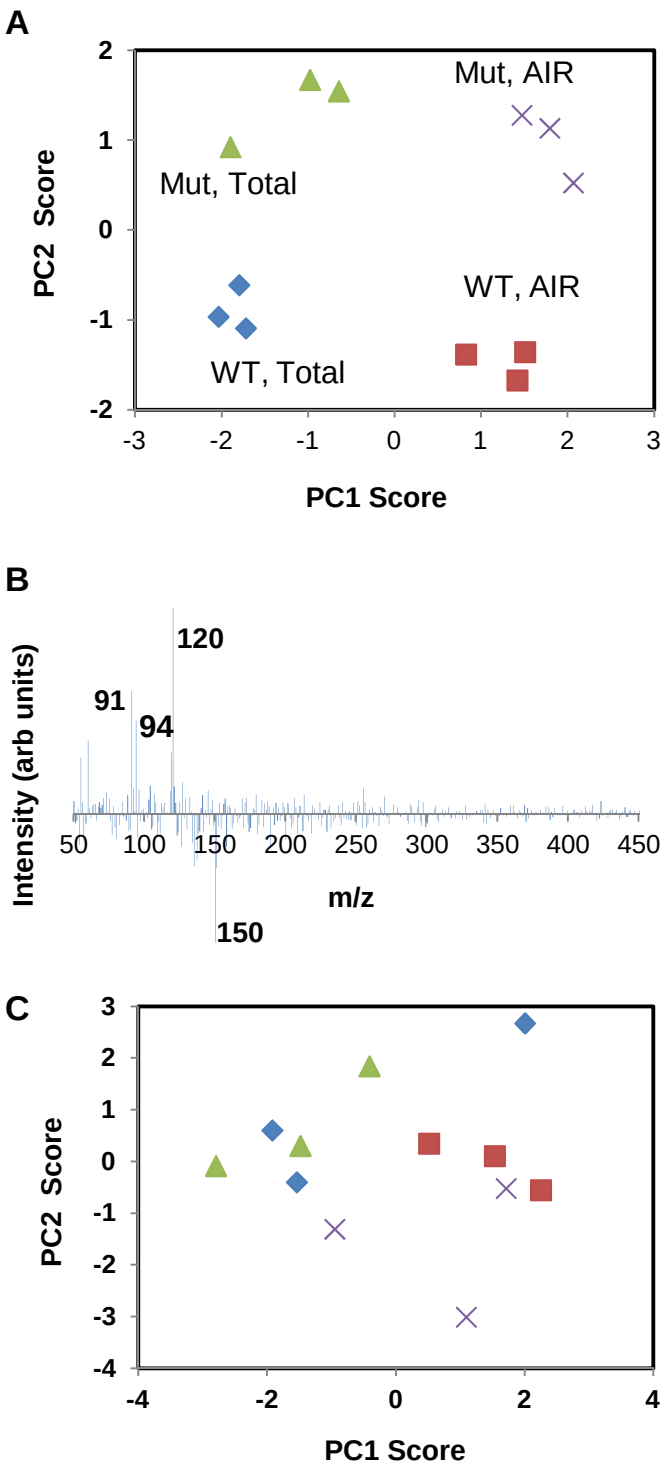

Figure 10. Principal component analysis of pyrolysis-molecular beam-mass spectrometry data for *OsAT10D-1* corroborates the change in extractable phenolics, but shows no difference in lignin composition. **(A)** First two components for technical replicates of total biomass (negative in principal component (PC) 1) and AIR (positive in PC1) for wild-type straw (WT, diamonds and squares, progeny of 4A-03423.5) and mutant straw (Mut, triangles and X's, progeny of 4A-03423.1). **(B)** Loadings plot for PC2 of (A). The mass to charge ratios of the four most differentially abundant ions are shown. The ions that are overrepresented in mutant tissue are 120 (4-vinylphenol or 2,3-dihydrobenzofuran), 91 (fragment of 2,3-dihydrobenzofuran and most phenols) and 94 (phenol). The ion that is most underrepresented in the mutant is 150 (coumaryl alcohol/coniferyl alcohol). **(C)** PCA for mutant and wild type residue after 2 N NaOH extraction. Samples are poorly distinguished indicating that the principle components of variation are extractable and, therefore, are not polymeric lignin.

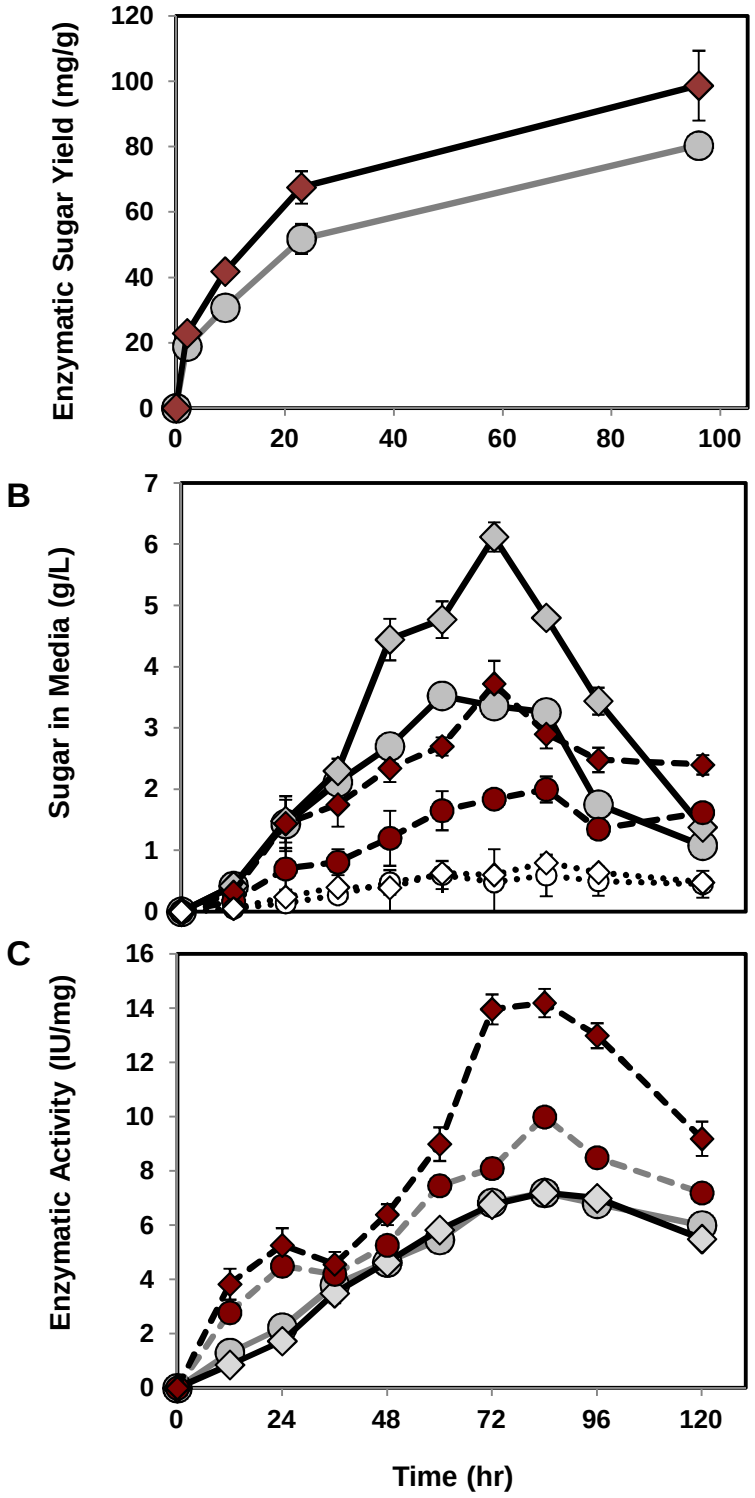

Figure 11. *OsAT10-D1* exhibits increased enzymatic and fungal deconstructability. **(A)** An enzyme cocktail of cellulase and ß-glucosidase releases more sugar from destarched AIR from mature straw of *OsAT10-D1* (red diamonds, *4A-03423.5* progeny) than from that of wild-type (light grey circles, *4A-03423.1* progeny). AIR was pretreated at 100 degrees for one hour at pH 5.5 prior to addition of enzyme. Error bars show the values of two technical replicates. **(B)** *Penicillium sp.* YT02 releases greater amounts of sugar from rice straw of *OsAT10-D1* (diamonds, *4A-03423.5* progeny) than from wild-type straw (circles, *4A-03423.1* progeny) pretreated via acid-explosion. Grey symbols indicate glucose, red symbols xylose, and white symbols arabinose. Error bars show 2*SEM of five replicate cultures. Raw values and difference data are provided in Supplemental Table III. **(C)** Xylanase activity (dashed lines, red symbols) in the fungal-straw slurry is enhanced in the presence of the mutant straw (diamonds) relative to in the wild-type straw (circles); whereas, carboxymethyl cellulase actitvity (solid lines, grey symbols) is unchanged. IU is nmoles of sugar per minute per mL. Error bars show 2*SEM of five replicate cultures.